Metabolic Engineering 47 (2018) 401–413

Contents lists available at ScienceDirect

Metabolic Engineering

journal homepage: www.elsevier.com/locate/meteng

Metabolic engineering to enhance heterologous production of hyaluronic acid in *Bacillus subtilis*

Adam W. Westbrook, Xiang Ren, Jaewon Oh, Murray Moo-Young, C. Perry Chou*

Department of Chemical Engineering, University of Waterloo, Waterloo, Ontario, Canada N2L 5B6

ARTICLE INFO

Keywords:
Metabolic engineering
Hyaluronic acid
Hyaluronan
CRISPR
Bacillus subtilis
Transcriptional interference

ABSTRACT

Hyaluronic acid (HA) is a high-value biopolymer that is produced in large scales using attenuated strains ofgroup C streptococci. However, due to the pathogenicity and fastidious nature of these bacteria, the development of bioprocesses for HA production centered on robust 'Generally Recognized as Safe (GRAS)' organisms, such as *Bacillus subtilis*, is of increased interest. Here, we report metabolic engineering of novel *B. subtilis* strains in which the carbon flux has been partially diverted from central metabolism, i.e. the pentose phosphate pathway (PPP) and glycolysis, into HA biosynthesis. First, an improved base strain of *B. subtilis* was engineered for more effective HA production with less susceptibility to catabolite repression when expressing genes from a xylose-inducible promoter. Subsequently, Clustered Regularly Interspaced Palindromic Repeats interference (CRISPRi) was applied to reduce the expression of individual *pfkA* or *zwf* in the base strain, leading to substantial improvements to the HA titer with a concomitant decrease in the molecular weight (MW). On the other hand, multiplexed repression of both *pfkA* and *zwf* expression resulted in increases to the HA titer of up to 108% and enhancements to the MW, compared to the base strain. Moreover, the addition of exogenous HA monomers, i.e. glucuronic acid (GlcUA) and *N*-acetyl-glucosamine (GlcNAc), to *B. subtilis* cultures markedly improved the HA MW but decreased the HA titer, providing insights into the mechanism of HA biosynthesis by streptococcal hyaluronan synthase (SeHAS) in *B. subtilis*. Our study demonstrates the successful application of metabolic engineering strategies to establish *B. subtilis* as an effective platform for high-level HA production.

1. Introduction

Hyaluronic acid (HA) is a linear, unbranched glycosaminoglycan composed of alternating *N*-acetyl-glucosamine (GlcNAc) and glucuronic acid (GlcUA) monomers joined by β−1,4 and β–1,3 linkages (Weissmann and Meyer, 1954). The biocompatibility and absence of immunogenicity of HA, and its unique rheological properties and hygroscopicity have led to its use in the biomedical, pharmaceutical, food, and cosmetic industries (Goa and Benfield, 1994; Kogan et al., 2007; Liu et al., 2011). The extraction of HA from animal sources, such as rooster combs, has gradually been replaced by microbial synthesis via attenuated strains of group C streptococci (i.e. *Streptococcus equisimilis* and *Streptococcus zooepidemicus*) (Liu et al., 2011). However, HA produced from *Streptococcus* sp. may contain exotoxins inherent to these pathogenic species (Widner et al., 2005), such that the adoption of production hosts with the 'Generally Recognized as Safe (GRAS)' designation by the Food and Drug Administration, USA, is highly attractive. (Liu et al., 2011). Heterologous HA production has been achieved in *Escherichia coli* (Mao et al., 2009; Yu and Stephanopoulos, 2008), *Lactococcus lactis* (Chien and Lee, 2007b; Prasad et al., 2010), *Agrobacterium* sp. (Mao and Chen, 2007), *Streptomyces albulus* (Yoshimura et al., 2015), *Corynebacterium glutamicum* (Cheng et al., 2017), *and Bacillus subtilis* (Chien and Lee, 2007a; Jia et al., 2013; Jin et al., 2016; Widner et al., 2005). In particular, *B. subtilis* shows considerable promise as it is genetically tractable, grows rapidly in simple media, has been granted GRAS status (Schallmey et al., 2004), and has been explored for large-scale production of HA (Liu et al., 2011).

In light of significant advances in the areas of synthetic biology, metabolic engineering, and molecular biology, strain engineering to enhance target metabolite production has become increasingly common (Keasling, 2010). The standard approach begins with the rational design of a biosynthetic pathway to generate the desired product. Heightened expression of key genes, in parallel with inactivation of genes in competing pathways, aims to direct carbon flux toward target metabolite formation (Lee et al., 2012). However, complete inactivation of certain essential genes associated with central metabolism or core aspects of physiology (e.g. ATP generation, cell division, etc.) may not be feasible, such that reducing expression levels of these genes,

* Corresponding author.
E-mail address: cpchou@uwaterloo.ca (C.P. Chou).

https://doi.org/10.1016/j.ymben.2018.04.016
Received 4 November 2017; Received in revised form 3 April 2018; Accepted 20 April 2018
Available online 23 April 2018

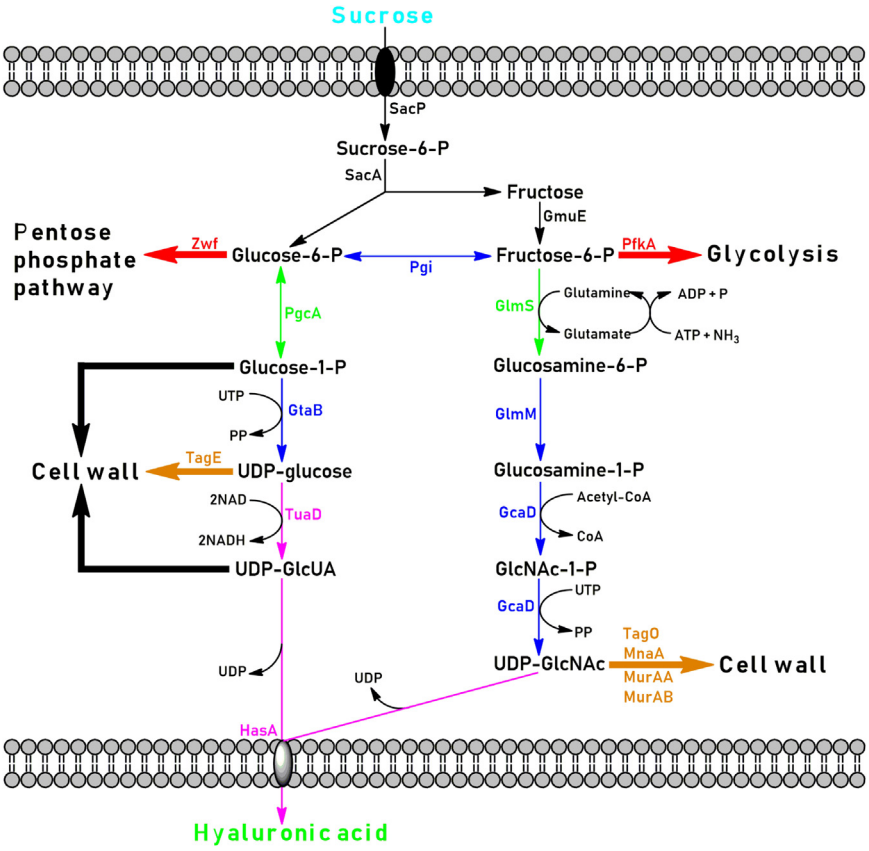

Fig. 1. The HA biosynthetic pathway in *B. subtilis*. Pink arrows: upregulated in all strains. Green arrows: upregulated in certain strains. Blue arrows: potential targets for upregulation. Red arrows: downregulated in certain strains. Orange arrows: potential targets for downregulation. Enzymes listed by category: TuaD, UDP-glucose 6-dehydrogenase; HasA, hyaluronan synthase; PgcA, phosphoglucomutase; GlmS, glutamine-fructose-6-P amidotransferase; Pgi, glucose-6-P isomerase; GtaB, UTP-glucose-1-P uridylyltransferase; GlmM, phosphoglucosamine mutase; GcaD, UDP-GlcNAc pyrophosphorylase; Zwf, glucose-6-P 1-dehydrogenase; PfkA, 6-phosphofructokinase; TagE, UDP-glucose: polyglycerol phosphate glucosyltransferase; TagO, UDP-GlcNAc: undecaprenyl-P N-acetylglucosaminyl-1-P transferase; MnaA, UDP-N-acetylmannosamine (ManNAc) 2-epimerase; MurAA, UDP-GlcNAc 1-carboxyvinyltransferase; MurAB, UDP-GlcNAc 1-carboxyvinyltransferase; SacP, phosphotransferase system sucrose-specific transporter; SacA, sucrose-6-P hydrolase; GmuE, fructokinase.

while maintaining cell physiology, may ultimately prove more effective (Desai and Papoutsakis, 1999). Prior efforts to produce HA in *B. subtilis* have primarily involved overexpressing genes comprising the HA biosynthetic pathway (Fig. 1). In the first demonstration, it was shown that uridine diphosphate (UDP)-GlcUA is limiting for HA biosynthesis, such that coexpression of *tuaD* (encoding native UDP-glucose-6 dehydrogenase; TuaD) and *seHas* (encoding hyaluronan synthase from *S. equisimilis*; SeHAS) was critical for high-level HA production (Widner et al., 2005). Coexpression of additional native enzymes involved in cell wall biosynthesis, i.e. uridine triphosphate (UTP)-glucose-1-P uridylyltransferase (GtaB; encoded by *gtaB*) and UDP-GlcNAc pyrophosphorylase (GcaD; encoded by *gcaD*), moderately improved HA production. Coexpression of *szHas* (encoding hyaluronan synthase from *S. zooepidemicus*; SzHAS), *tuaD*, and *vhb* (encoding hemoglobin from *Vitreoscilla*; VHb), significantly improved HA production, presumably due to increased ATP production resulting from *vhb* expression (Chien and Lee, 2007a). Recently, various combinations of genes in the HA biosynthetic pathway were overexpressed (Jin et al., 2016). The coexpression of *szHas*, *tuaD*, *gtaB*, *glmS* (encoding native L-glutamine-D-fructose-6-phosphate amidotransferase; GlmS), *glmM* (encoding native phosphoglucosamine mutase; GlmM), and *gcaD* improved the HA titer by ~30%, compared to the coexpression of only *szHas* and *tuaD*, or *szHas* and *gcaD*, without improving the MW. On the other hand, simply downregulating expression of *pfkA* (encoding 6-phosphofructokinase; PfkA), via replacement of the native ATG start codon with TTG, moderately improved HA production (Jin et al., 2016). Moreover, the carbon source used to produce HA in *B. subtilis* can affect the MW (Westbrook et al., 2016), and modifying the cardiolipin content and distribution in the cell membrane can improve both the titer and MW (Westbrook et al., 2018a). Collectively, the results from prior studies of HA production in *B. subtilis* suggest that coexpressing key genes from the HA biosynthetic pathway results in diminishing returns on the titer and MW, while metabolic engineering strategies, such as enhancing ATP generation or reducing glycolytic flux, have a greater impact on culture performance by reducing the burden on cellular resources.

Heterologous HA production directly competes with central metabolism and cell wall biosynthesis, making it particularly challenging to manipulate with metabolic engineering strategies. In *B. subtilis*, glucose-6-P enters the branch point between the pentose phosphate pathway (PPP), glycolysis, and the synthesis of cell wall components (Fig. 1). Glucose-6-P 1-dehydrogenase (Zwf; encoded by *zwf*) converts glucose-6-P to 6-phosphogluconolactone to initiate the oxidative branch of the PPP. In opposing directions, phosphoglucomutase (PgcA; encoded by *pgcA*) and glucose-6-P isomerase (Pgi; encoded by *pgi*) convert glucose-6-P to glucose-1-P and fructose-6-P, respectively. Glucose-1-P feeds into the synthesis of cell wall components (e.g. teichoic and teichuronic acids), and fructose-6-P will enter glycolysis upon conversion to fructose-1,6-bisphosphate by PfkA, or be converted to glucosamine-6-P, an intermediate in the synthesis of peptidoglycan and other cell wall constituents, by GlmS. Streptococcal Class I HAS alternately adds UDP-GlcNAc and UDP-GlcUA, intermediates in the synthesis of cell wall components respectively derived from glucosamine-6-P and glucose-1-P, to the reducing end of the growing HA chain (Weigel et al., 1997). Presumably, shifting carbon flux from central metabolism toward cell wall biosynthesis may improve HA production though cell physiology may be affected. In fact, inactivation of *pfkA* was lethal to *B. subtilis* (Fischer and Sauer, 2005; Kobayashi et al., 2003), and inactivation of *zwf* led to significant carbon flux rerouting into glycolysis (Fischer and Sauer, 2005). Accordingly, repression of *pfkA* and/or *zwf* expression may be an effective approach to redirect carbon flux from glycolysis and the PPP, respectively, toward cell wall biosynthesis and, ultimately, HA biosynthesis with minimum impact to cell physiology.

Table 1
Strains and plasmids used in this study.

Strain or plasmid	*Characteristics*[a]	Source
E. coli HI-Control™ 10G	*mcrA* Δ(*mrr-hsdRMS-mcrBC*) *endA1 recA1* ϕ80d*lacZ*ΔM15 Δ*lacX74 araD139* Δ (*ara,leu*)7697*galU galK rpsL* (StrR) *nupG* λ–*tonA* Mini-F *lacIq1* (Gent^R)	Lucigen
B. subtilis		
1A751	*his npr*R2 *npr*E18 Δ*apr*A3 Δ*egl*S102 Δ*bgl*T *bgl*SRV	(Wolf et al., 1995)
AW008	1A751 *amyE*::(P_{grac}::*seHas*:*tuaD*, Neo^R)	(Westbrook et al., 2018a)
AW009	1A751 *amyE*::($P_{grac.\ UPmod}$::*seHas*:*tuaD*, Neo^R),	This work
AW014-2	1A751 *amyE*::($P_{grac.UPmod}$::*seHas*:*tuaD*, Neo^R) *lacA*::($P_{xylA,\ Bm}$::*dcas9*, *xylR*, Erm^R)	(Westbrook et al., 2016)
AW016-2	1A751 *amyE*::($P_{grac.UPmod}$::*seHas*:*tuaD*, Neo^R) *lacA*::($P_{xylA,\ Bm}$::*dcas9*, *xylR*, Erm^R), *wprA*::($P_{xylA.SphI+1}$::*lacZ*-gRNA.P28NT), *ugtP*::(*lacI*, P_{grac}::*lacZ*, Spc^R)	(Westbrook et al., 2016)
AW001-3	1A751 *amyE*::($P_{grac.UPmod}$::*seHas*:*tuaD*, Neo^R) *lacA*::($P_{xylA,\ Bm}$::*dcas9*, *xylR*, Erm^R) *vpr*::($P_{grac.UPmod}$::*araE*)	This work
AW002-3	1A751 *amyE*::($P_{grac.UPmod}$::*seHas*:*tuaD*, Neo^R) *lacA*::($P_{xylA,\ Bm}$::*dcas9*, *xylR*, Erm^R) *vpr*::($P_{grac.\Delta UP}$::*araE*)	This work
AW003–3	1A751 *amyE*::($P_{grac.UPmod}$::*seHas*:*tuaD*, Neo^R) *lacA*::($P_{xylA,\ Bm}$::*dcas9*, *xylR*, Erm^R) *vpr*::($P_{grac.\Delta UP}$::*araE*) *wprA*::($P_{xylA.SphI+1}$::*lacZ*-gRNA.P28NT)	This work
AW004-3	1A751 *amyE*::($P_{grac.UPmod}$::*seHas*:*tuaD*, Neo^R) *lacA*::($P_{xylA,\ Bm}$::*dcas9*, *xylR*, Erm^R) *vpr*::($P_{grac.\Delta UP}$::*araE*) *wprA*::($P_{xylA.SphI+1}$::*lacZ*-gRNA.P28NT) *ugtP*::(*lacI*, P_{grac}::*lacZ*, Spc^R)	This work
AW005-3	1A751 *amyE*::($P_{grac.UPmod}$::*seHas*:*tuaD*, Neo^R) *lacA*::($P_{xylA,\ Bm}$::*dcas9*, *xylR*, Erm^R) *vpr*::($P_{grac.\Delta UP}$::*araE*) *wprA*::($P_{xylA.SphI+1}$::*pfkA*-gRNA.P41NT, *araR*, P_{araE}::*mazF*, Spc^R)	This work
AW006-3	1A751 *amyE*::($P_{grac.UPmod}$::*seHas*:*tuaD*, Neo^R) *lacA*::($P_{xylA,\ Bm}$::*dcas9*, *xylR*, Erm^R) *vpr*::($P_{grac.\Delta UP}$::*araE*) *wprA*::($P_{xylA.SphI+1}$::*pfkA*-gRNA.P41NT(10C-A), *araR*, P_{araE}::*mazF*, Spc^R)	This work
AW007-3	1A751 *amyE*::($P_{grac.UPmod}$::*seHas*:*tuaD*, Neo^R) *lacA*::($P_{xylA,\ Bm}$::*dcas9*, *xylR*, Erm^R) *vpr*::($P_{grac.\Delta UP}$::*araE*) *wprA*::($P_{xylA.SphI+1}$::*pfkA*-gRNA.P41NT(15U-C), *araR*, P_{araE}::*mazF*, Spc^R)	This work
AW008-3	1A751 *amyE*::($P_{grac.UPmod}$::*seHas*:*tuaD*, Neo^R) *lacA*::($P_{xylA,\ Bm}$::*dcas9*, *xylR*, Erm^R) *vpr*::($P_{grac.\Delta UP}$::*araE*) *wprA*::($P_{xylA.SphI+1}$::*pfkA*-gRNA.P315NT(10G-A), *araR*, P_{araE}::*mazF*, Spc^R)	This work
AW009-3	1A751 *amyE*::($P_{grac.UPmod}$::*seHas*:*tuaD*, Neo^R) *lacA*::($P_{xylA,\ Bm}$::*dcas9*, *xylR*, Erm^R) *vpr*::($P_{grac.\Delta UP}$::*araE*) *wprA*::($P_{xylA.SphI+1}$::*pfkA*-gRNA.P315NT(15U-G), *araR*, P_{araE}::*mazF*, Spc^R)	This work
AW010-3	1A751 *amyE*::($P_{grac.UPmod}$::*seHas*:*tuaD*, Neo^R) *lacA*::($P_{xylA,\ Bm}$::*dcas9*, *xylR*, Erm^R) *vpr*::($P_{grac.\Delta UP}$::*araE*) *wprA*::($P_{xylA.SphI+1}$::*pfkA*-gRNA.P610NT(10G-A), *araR*, P_{araE}::*mazF*, Spc^R)	This work
AW011-3	1A751 *amyE*::($P_{grac.UPmod}$::*seHas*:*tuaD*, Neo^R) *lacA*::($P_{xylA,\ Bm}$::*dcas9*, *xylR*, Erm^R) *vpr*::($P_{grac.\Delta UP}$::*araE*) *wprA*::($P_{xylA.SphI+1}$::*pfkA*-gRNA.P610NT(15U-C), *araR*, P_{araE}::*mazF*, Spc^R)	This work
AW012-3	1A751 *amyE*::($P_{grac.UPmod}$::*seHas*:*tuaD*, Neo^R) *lacA*::($P_{xylA,\ Bm}$::*dcas9*, *xylR*, Erm^R) *vpr*::($P_{grac.\Delta UP}$::*araE*) *wprA*::($P_{xylA.SphI+1}$::*zwf*-gRNA.P92NT, *araR*, P_{araE}::*mazF*, Spc^R)	This work
AW013-3	1A751 *amyE*::($P_{grac.UPmod}$::*seHas*:*tuaD*, Neo^R) *lacA*::($P_{xylA,\ Bm}$::*dcas9*, *xylR*, Erm^R) *vpr*::($P_{grac.\Delta UP}$::*araE*) *wprA*::($P_{xylA.SphI+1}$::*zwf*-gRNA.P92NT(10U-G), *araR*, P_{araE}::*mazF*, Spc^R)	This work
AW014-3	1A751 *amyE*::($P_{grac.UPmod}$::*seHas*:*tuaD*, Neo^R) *lacA*::($P_{xylA,\ Bm}$::*dcas9*, *xylR*, Erm^R) *vpr*::($P_{grac.\Delta UP}$::*araE*) *wprA*::($P_{xylA.SphI+1}$::*zwf*-gRNA.P92NT(15C-A), *araR*, P_{araE}::*mazF*, Spc^R)	This work
AW015-3	1A751 *amyE*::($P_{grac.UPmod}$::*seHas*:*tuaD*, Neo^R) *lacA*::($P_{xylA,\ Bm}$::*dcas9*, *xylR*, Erm^R) *vpr*::($P_{grac.\Delta UP}$::*araE*) *wprA*::($P_{xylA.SphI+1}$::*zwf*-gRNA.P603NT, *araR*, P_{araE}::*mazF*, Spc^R)	This work
AW016-3	1A751 *amyE*::($P_{grac.UPmod}$::*seHas*:*tuaD*, Neo^R) *lacA*::($P_{xylA,\ Bm}$::*dcas9*, *xylR*, Erm^R) *vpr*::($P_{grac.\Delta UP}$::*araE*) *wprA*::($P_{xylA.SphI+1}$::*zwf*-gRNA.P603NT(10U-C), *araR*, P_{araE}::*mazF*, Spc^R)	This work
AW017-3	1A751 *amyE*::($P_{grac.UPmod}$::*seHas*:*tuaD*, Neo^R) *lacA*::($P_{xylA,\ Bm}$::*dcas9*, *xylR*, Erm^R) *vpr*::($P_{grac.\Delta UP}$::*araE*) *wprA*::($P_{xylA.SphI+1}$::*zwf*-gRNA.P603NT(15G-U), *araR*, P_{araE}::*mazF*, Spc^R)	This work
AW018-3	1A751 *amyE*::($P_{grac.UPmod}$::*seHas*:*tuaD*, Neo^R) *lacA*::($P_{xylA,\ Bm}$::*dcas9*, *xylR*, Erm^R) *vpr*::($P_{grac.\Delta UP}$::*araE*) *wprA*::($P_{xylA.SphI+1}$::*zwf*-gRNA.P603NT(10U-C), $P_{xylA.SphI+1}$::*pfkA*-gRNA.P41NT, *araR*, P_{araE}::*mazF*, Spc^R)	This work
AW019-3	1A751 *amyE*::($P_{grac.UPmod}$::*seHas*:*tuaD*, Neo^R) *lacA*::($P_{xylA,\ Bm}$::*dcas9*, *xylR*, Erm^R) *vpr*::($P_{grac.\Delta UP}$::*araE*) *wprA*::($P_{xylA.SphI+1}$::*zwf*-gRNA.P603NT(10U-C), $P_{xylA.SphI+1}$::*pfkA*-gRNA.P41NT(10C-A), *araR*, P_{araE}::*mazF*, Spc^R)	This work
AW020-3	1A751 *amyE*::($P_{grac.\ UPmod}$::*seHas*:*tuaD*, Neo^R) *thrC*::(P_{grac}::*pgcA*)	This work
AW021-3	1A751 *amyE*::($P_{grac.\ UPmod}$::*seHas*:*tuaD*, Neo^R) *thrC*::(P_{grac}::*glmS*)	This work
AW022-3	1A751 *amyE*::($P_{grac.\ UPmod}$::*seHas*:*tuaD*, Neo^R) *thrC*::(P_{grac}::*pgcA*:*glmS*)	This work
Plasmids		
pHT01	*lacI*, P_{grac}, Cat^R, Amp^R, *B. subtilis* replicating shuttle vector	(Nguyen et al., 2007)
pAW008	P_{grac}::*seHas*:*tuaD*, Neo^R, *B. subtilis amyE* integration vector	(Westbrook et al., 2016)
pAW009	$P_{grac.UPmod}$::*seHas*:*tuaD*, Neo^R, *B. subtilis amyE* integration vector	This work
pAW016	P_{grac}::*lacZ*, *lacI*, Spc^R, Erm^R, *B. subtilis ugtP* integration vector	(Westbrook et al., 2016)
pAW017-2	$P_{xylA.SphI+1}$, P_{araE}::*mazF*, *araR*, Spc^R, Erm^R, *B. subtilis* auto-evicting counter-selectable *wprA* integration vector	(Westbrook et al., 2016)
pAW018-2	$P_{xylA.SphI+1}$::*lacZ*-gRNA.P28NT, P_{araE}::*mazF*, *araR*, Spc^R, Erm^R, *B. subtilis* auto-evicting counter-selectable *wprA* integration vector	(Westbrook et al., 2016)
pAW019-2	$P_{xylA,\ Bm}$::*dcas9*, *xylR*, Amp^R, Erm^R *B. subtilis lacA* integration vector	(Westbrook et al., 2016)
pAW002-4	P_{grac}::*pgsA*:*clsA*, P_{araE}::*mazF*, *araR*, Spc^R, Erm^R, *B. subtilis* auto-evicting counter-selectable *thrC* integration vector	(Westbrook et al., 2018a)
pAW001-3	$P_{grac.UPmod}$::*araE*, P_{araE}::*mazF*, *araR*, Spc^R, Erm^R, *B. subtilis* auto-evicting counter-selectable *vpr* integration vector	This work
pAW002-3	$P_{grac.\Delta UP}$::*araE*, P_{araE}::*mazF*, *araR*, Spc^R, Erm^R, *B. subtilis* auto-evicting counter-selectable *vpr* integration vector	This work
pAW003-3	$P_{xylA.SphI+1}$::*pfkA*-gRNA.P41NT, P_{araE}::*mazF*, *araR*, Spc^R, Erm^R, *B. subtilis* auto-evicting counter-selectable *wprA* integration vector	This work
pAW004-3	$P_{xylA.SphI+1}$::*pfkA*-gRNA.P41NT(10C-A), P_{araE}::*mazF*, *araR*, Spc^R, Erm^R, *B. subtilis* auto-evicting counter-selectable *wprA* integration vector	This work
pAW005-3	$P_{xylA.SphI+1}$::*pfkA*-gRNA.P41NT(15U-C), P_{araE}::*mazF*, *araR*, Spc^R, Erm^R, *B. subtilis* auto-evicting counter-selectable *wprA* integration vector	This work
pAW006-3	$P_{xylA.SphI+1}$::*pfkA*-gRNA.P315NT(10G-A), P_{araE}::*mazF*, *araR*, Spc^R, Erm^R, *B. subtilis* auto-evicting counter-selectable *wprA* integration vector	This work
pAW007-3	$P_{xylA.SphI+1}$::*pfkA*-gRNA.P315NT(15U-G), P_{araE}::*mazF*, *araR*, Spc^R, Erm^R, *B. subtilis* auto-evicting counter-selectable *wprA* integration vector	This work
pAW008-3	$P_{xylA.SphI+1}$::*pfkA*-gRNA.P610NT(10G-A), P_{araE}::*mazF*, *araR*, Spc^R, Erm^R, *B. subtilis* auto-evicting counter-selectable *wprA* integration vector	This work
pAW009-3	$P_{xylA.SphI+1}$::*pfkA*-gRNA.P610NT(15U-C), P_{araE}::*mazF*, *araR*, Spc^R, Erm^R, *B. subtilis* auto-evicting counter-selectable *wprA* integration vector	This work

(*continued on next page*)

Table 1 (*continued*)

Strain or plasmid	*Characteristics*[a]	Source
pAW010-3	$P_{xylA.SphI+1}$::*zwf*-gRNA.P92NT, P_{araE}::*mazF*, *araR*, Spc^R, Erm^R, *B. subtilis* auto-evicting counter-selectable *wprA* integration vector	This work
pAW011-3	$P_{xylA.SphI+1}$::*zwf*-gRNA.P92NT(10U-G), P_{araE}::*mazF*, *araR*, Spc^R, Erm^R, *B. subtilis* auto-evicting counter-selectable *wprA* integration vector	This work
pAW012-3	$P_{xylA.SphI+1}$::*zwf*-gRNA.P92NT(15C-A), P_{araE}::*mazF*, *araR*, Spc^R, Erm^R, *B. subtilis* auto-evicting counter-selectable *wprA* integration vector	This work
pAW013-3	$P_{xylA.SphI+1}$::*zwf*-gRNA.P603NT, P_{araE}::*mazF*, *araR*, Spc^R, Erm^R, *B. subtilis* auto-evicting counter-selectable *wprA* integration vector	This work
pAW014-3	$P_{xylA.SphI+1}$::*zwf*-gRNA.P603NT(10U-C), P_{araE}::*mazF*, *araR*, Spc^R, Erm^R, *B. subtilis* auto-evicting counter-selectable *wprA* integration vector	This work
pAW015-3	$P_{xylA.SphI+1}$::*zwf*-gRNA.P603NT(15G-U), P_{araE}::*mazF*, *araR*, Spc^R, Erm^R, *B. subtilis* auto-evicting counter-selectable *wprA* integration vector	This work
pAW016-3	(*Bgl*II) $P_{xylA.SphI+1}$, P_{araE}::*mazF*, *araR*, Spc^R, Erm^R, *B. subtilis* multi-gRNA counter-selectable *wprA* integration vector	This work
pAW017-3	(*Bgl*II) $P_{xylA.SphI+1}$::*zwf*-gRNA.P603NT(10U-C), $P_{xylA.SphI+1}$::*pfkA*-gRNA.P41NT, P_{araE}::*mazF*, *araR*, Spc^R, Erm^R, *B. subtilis* multi-gRNA counter-selectable *wprA* integration vector	This work
pAW018-3	(*Bgl*II) $P_{xylA.SphI+1}$::*zwf*-gRNA.P603NT(10U-C), $P_{xylA.SphI+1}$::*pfkA*-gRNA.P41NT(10C-A), P_{araE}::*mazF*, *araR*, Spc^R, Erm^R, *B. subtilis* multi-gRNA counter-selectable *wprA* integration vector	This work
pAW019-3	P_{grac}::*pgcA*, P_{araE}::*mazF*, *araR*, Spc^R, Erm^R, *B. subtilis* auto-evicting counter-selectable *thrC* integration vector	This work
pAW020-3	P_{grac}::*glmS*, P_{araE}::*mazF*, *araR*, Spc^R, Erm^R, *B. subtilis* auto-evicting counter-selectable *thrC* integration vector	This work
pAW021-3	P_{grac}::*pgcA*:*glmS*, P_{araE}::*mazF*, *araR*, Spc^R, Erm^R, *B. subtilis* auto-evicting counter-selectable *thrC* integration vector	This work

[a] *amyE*: α-amylase; *araE*: transporter of L-arabinose and D-xylose; *araR*: repressor of arabinose operons; d*cas9*: dead Cas9 (derived from *S. pyogenes*); *glmS*: L-glutamine-D-fructose-6-phosphate amidotransferase; *lacA* (*ganA*): β-galactosidase; *lacI*: lactose operon repressor (*E. coli*); *lacZ*: β-galactosidase (*E. coli*); *mazF*: endoribonuclease (*Escherichia coli*); *pfkA*: 6-phosphofructokinase; *pgcA*: phosphoglucomutase; *thrC*: threonine synthase; *ugtP*: UDP-glucose diacylglyceroltransferase; *seHas*: hyaluronan synthase (*Streptococcus equisimilis*); *tuaD*: UDP-glucose 6-dehydrogenase; *xylR*: xylose operon repressor (*Bacillus megaterium*); *wprA*: cell wall-associated protease; *zwf*: glucose-6-phosphate 1-dehydrogenase; Neo^R: neomycin resistance cassette; Erm^R: erythromycin resistance cassette; Spc^R: spectinomycin resistance cassette; Amp^R: ampicillin resistance cassette.

2. Materials and methods

2.1. Bacterial strains, primers and plasmids

The *B. subtilis* strains used in this study are listed in Table 1. *E. coli* HI-Control™ 10 G chemically competent cells (Lucigen; Wisconsin, USA) were prepared as electrocompetent cells as described previously (Sambrook and Russell, 2001) and used as host for plasmid construction. *B. subtilis* and *E. coli* strains were maintained as glycerol stocks at −80 °C. Primers (Table S1) were synthesized by Integrated DNA Technologies (Iowa, USA).

2.2. Plasmid construction

DNA manipulation was performed using standard cloning techniques (Sambrook and Russell, 2001), and DNA sequencing was conducted by The Centre for Applied Genomics (Ontario, Canada). To construct pAW009, promoter $P_{grac.\ UPmod}$ (i.e. promoter P61), a weaker derivative of promoter P_{grac} (i.e. promoter P01) for which the relative promoter strength is ~0.5 (Phan et al., 2012), was amplified from pHT01 (Nguyen et al., 2007) with primers P97/P98, and inserted into *Sal*I/*Bam*HI digested pAW008 (Westbrook et al., 2016). Transformation of pAW009 into *B. subtilis* results in the integration of a $P_{grac.UPmod}$::*seHas*:*tuaD* cassette at the *amyE* locus (Fig. 2). To construct the expression cassette in which *araE*, encoding the broad specificity transporter of L-arabinose and D-xylose (AraE) (Krispin and Allmansberger, 1998), was driven by promoter $P_{grac.UPmod}$ from the *vpr* locus, $P_{grac.UPmod}$ was amplified with primers P114/P115 from pHT01, *araE* was amplified with primers P116/P117 from 1A751 genomic DNA (gDNA), and the two fragments were spliced via Splicing by Overlap Extension (SOE)-PCR (this process will be subsequently referred to as splicing), generating a $P_{grac.UPmod}$::*araE* cassette. The *vpr* homology length (HL) − 5' was then amplified with primers P118/P119 and spliced with the $P_{grac.UPmod}$::*araE* cassette, yielding a *vpr* HL-5'-$P_{grac.UPmod}$::*araE* cassette, which was subsequently inserted into SbfI/AsiSI-digested pAW002–4 (Westbrook et al., 2018a). To complete the vector, the *vpr* HL-3' was amplified with primers P120/P121 from 1A751 gDNA and inserted in place of the *thrC* HL-3', yielding pAW001–3. To construct pAW002–3, promoter $P_{grac.\Delta UP}$ was amplified with primers P150/P151 from pAW009 and inserted into *Avr*II/*Sph*I-digested pAW001–3. $P_{grac.\Delta UP}$ (i.e. promoter P70) is a weaker derivative of P_{grac} for which the relative promoter strength is ~0.1 (Phan et al., 2012).

The gRNA cassettes *pfkA*-gRNA.P41NT, *pfkA*-gRNA.P41NT(10C-A), *pfkA*-gRNA.P41NT(15U-C), *pfkA*-gRNA.P315NT(10G-A), *pfkA*-gRNA.P315NT(15U-G), *pfkA*-gRNA.P610NT(10G-A), and *pfkA*-gRNA.P610NT(15U-C) were amplified with respective forward primers P107-P113 and common reverse primer P32 from pgRNA-bacteria (Qi et al., 2013), and inserted into *Sph*I/*Nco*I-digested pAW017-2 (Westbrook et al., 2016) to obtain respective gRNA delivery vectors pAW003-3, pAW004-3, pAW005-3, pAW006-3, pAW007-3, pAW008-3, and pAW009-3. The gRNA cassettes *zwf*-gRNA.P92NT, *zwf*-gRNA.P92NT(10U-G), *zwf*-gRNA.P92NT(15C-A), *zwf*-gRNA.P603NT, *zwf*-gRNA.P603NT(10U-C), and *zwf*-gRNA.P603NT(15G-U) were amplified with respective forward primers P152-P157 and common reverse primer P32 from pgRNA-bacteria, and inserted into *Sph*I/*Nco*I-digested pAW017-2 to obtain respective gRNA delivery vectors pAW010-3, pAW011-3, pAW012-3, pAW013-3, pAW014-3, and pAW015-3. To construct the multi-gRNA delivery vector, the *Bgl*II and *Bam*HI restriction sites upstream and downstream of *mazF*, respectively, were removed, and a new *Bgl*II restriction site was inserted between the *Nhe*I restriction site and promoter $P_{xylA.SphI+1}$ in pAW017-2 to facilitate Biobrick cloning of gRNA transcription cassettes as previously described (Westbrook et al., 2016). This was accomplished by amplifying the $P_{xylA.\ SphI+1}$-direct repeat (DR) cassette and *mazF* from pAW017-2 with primers P28/P158 (*Nhe*I/–) and P159/P31 (–/*Bam*HI), respectively, followed by splicing of the two fragments to generate a $P_{xylA.\ SphI+1}$-DR-*mazF* cassette, which was subsequently inserted into *Nhe*I/*Bgl*II digested pAW017-2, generating pAW016-3. The previously amplified *zwf*-gRNA.P603NT(10U-C) cassette was then inserted into *Sph*I/*Nco*I-digested pAW016-3. To complete the respective dual gRNA delivery vectors pAW017-3 and pAW018-3, the $P_{xylA.\ SphI+1}$::*pfkA*-gRNA.P41NT and $P_{xylA.\ SphI+1}$::*pfkA*-gRNA.P41NT(10C-A) cassettes were amplified with primers P28/P33 (*Nhe*I/*Bam*HI), and inserted into the *Nhe*I/*Bgl*II-digested derivative of pAW016-3 containing *zwf*-gRNA.P603NT(10U-C). All gRNA delivery vectors were linearized with

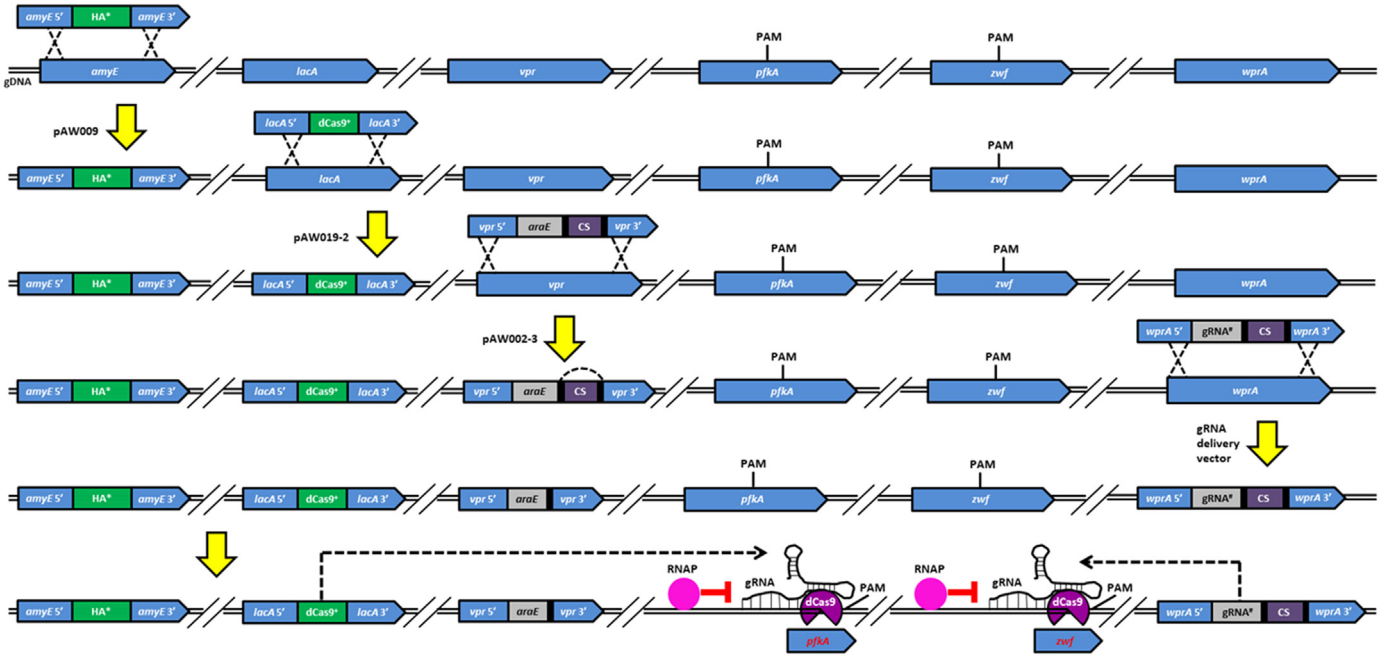

Fig. 2. Genomic engineering strategies to enhance HA production in *B. subtilis*. *B. subtilis* 1A751 was transformed with pAW009, yielding strain AW009, which synthesizes HA. AW009 was subsequently transformed with pAW019-2, yielding strain AW014-2, which expresses xylose-inducible dCas9. AW014-2 was then transformed with pAW002-3, and the combined P_{araE}::*mazF*-Spc^R (CS) cassette was subsequently auto-evicted via single-crossover recombination between the flanking direct repeats (black rectangles), yielding strain AW002-3, which constitutively expresses *araE* to enhance xylose uptake. To generate strains in which expression of *pfkA* was repressed, AW002-3 was transformed with various gRNA delivery vectors containing *pfkA*-targeting gRNAs. Similarly, to generate strains in which expression of *zwf* was repressed, AW002-3 was transformed with various gRNA delivery vectors containing *zwf*-targeting gRNAs. To generate strains in which expression of both *pfkA* and *zwf* were repressed, AW002-3 was transformed with pAW017-3 or pAW018-3, resulting in respective strains AW018-3 and AW019-3 that transcribe both *pfkA*- and *zwf*-targeting gRNAs. The gRNAs direct dCas9 to *pfkA* and/or *zwf* based on the presence of a PAM site and adjacent seed region complementary to the protospacer, and the dCas9-gRNA complex remains bound to the target, partially blocking transcription of *pfkA* and/or *zwf* by RNA polymerase (RNAP).

*Sac*I prior to transformation into *B. subtilis*.

To construct an expression cassette in which *pgcA* was driven by promoter P_{grac} from the *thrC* locus, the *thrC* HL-5'-P_{grac} cassette was amplified with primers P160/P161 from pAW002–4, *pgcA* was amplified with primers P162/P163 from 1A751 gDNA, and the two fragments were spliced, generating a *thrC* HL-5'-P_{grac}::*pgcA* cassette, which was subsequently inserted into SbfI/AsiSI digested pAW002–4, yielding pAW019-3. Similarly, to construct an expression cassette in which *glmS* was driven by promoter P_{grac} from the *thrC* locus, the *thrC* HL-5'-P_{grac} cassette was amplified with primers P160/P164 from pAW002–4, *glmS* was amplified with primers P165/P166 from 1A751 gDNA, and the two fragments were spliced, generating a *thrC* HL-5'-P_{grac}::*glmS* cassette, which was subsequently inserted into SbfI/AsiSI digested pAW002–4, yielding pAW020-3. Finally, to construct an expression cassette in which *pgcA* and *glmS* were driven by promoter P_{grac} from the *thrC* locus, *glmS* was amplified with primers P167/P166 from 1A751 gDNA, and was subsequently inserted into *Cla*I/AsiSI digested pAW019-3, yielding pAW021-3.

2.3. Competent cell preparation and transformation

Transformation of *B. subtilis* was performed using a standard protocol for natural competence (Harwood and Cutting, 1990). SpC medium contained the following (per L): $(NH_4)_2SO_4$, 1.67 g; K_2HPO_4, 11.64 g; KH_2PO_4, 5.0 g; trisodium citrate dihydrate, 833 mg; glucose, 4.17 g; $MgSO_4{\cdot}7H_2O$, 151 mg; yeast extract, 1.67 g; casamino acids, 208 mg; Arg, 7.5 g; His, 383 mg; Trp, 48 mg. SpII medium contained the following (per L): $(NH_4)_2SO_4$, 1.67 g; K_2HPO_4, 11.64 g; KH_2PO_4, 5.0 g; trisodium citrate dihydrate, 833 mg; glucose, 4.17 g; $MgSO_4{\cdot}7H_2O$, 725 mg; yeast extract, 858 mg; casamino acids, 86 mg; Arg, 3.78 g; His, 189 mg; Trp, 24 mg; $CaCl_2$, 48 mg. *B. subtilis* strains were plated on non-select lysogeny broth (LB) agar containing 5 g/L NaCl, 5 g/L yeast extract, 10 g/L tryptone, and 15 g/L agar, and incubated overnight. Pre-warmed SpC medium was inoculated by cell patches from the overnight plate to OD_{600} 0.5–0.7. Seventy five min after the logarithmic growth phase ended, cultured cells were then diluted 100-fold in pre-warmed SpII medium, and incubated for 110 min before harvesting. Transformed cells were incubated for 80 min at 260 revolutions per min (rpm), and then plated on LB agar containing 12 g/L glucose (LBG) and 85 μg/mL spectinomycin to select recombinants. To facilitate auto-eviction of the P_{araE}::*mazF*-Spc^R cassette after transformation of counter-selectable integration vectors, cells were grown for ~20 h in non-select LB at 37 °C and 260 rpm, plated on LB agar containing 20 g/L arabinose (LBA), and screened for spectinomycin sensitivity. All cultivation steps were conducted at 37 °C and 300 rpm unless otherwise indicated.

2.4. HA production, purification and analysis

HA production was assessed as previously described (Westbrook et al., 2016) with minor modifications. *B. subtilis* strains were plated on non-select LB and grown overnight at 37 °C. A single colony was used to inoculate 25 mL non-select LB, and the culture was grown for ~13 h at 37 °C and 280 rpm. The culture was then used to inoculate 20 mL pre-warmed non-select cultivation medium (4% v/v) of the following composition (per L): sucrose, 20 g; $(NH_4)_2SO_4$, 1 g; $K_2HPO_4{\cdot}3H_2O$, 9.15 g; KH_2PO_4, 3 g; trisodium citrate·$2H_2O$, 1 g; yeast extract, 10 g; casamino acids, 2.5 g; $CaCl_2$, 5.5 mg; $FeCl_2{\cdot}6H_2O$, 13.5 mg; $MnCl_2{\cdot}4H_2O$, 1 mg; $ZnCl_2$, 1.7 mg; $CuCl_2{\cdot}2H_2O$, 0.43 mg; $CoCl_2{\cdot}6H_2O$, 0.6 mg; $Na_2MoO_4{\cdot}2H_2O$, 0.6 mg. Cultures were grown at 37 °C and 280 rpm, and were induced with xylose (0.75% wt/v) 1.5 h after inoculation. Samples were diluted appropriately in phosphate buffered

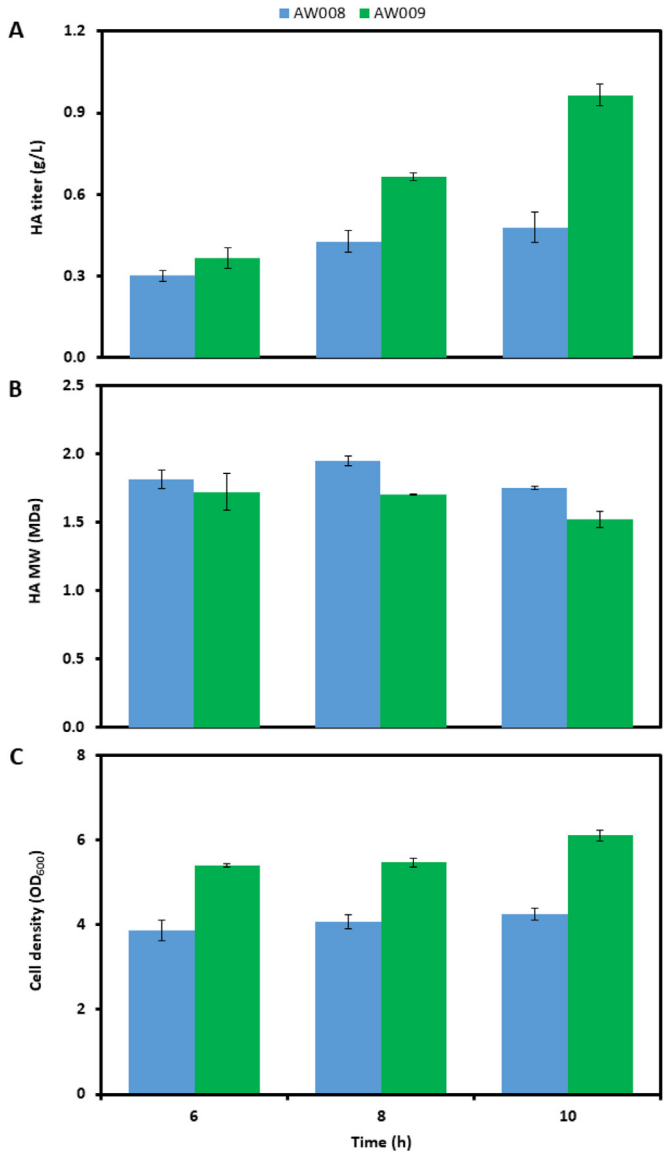

Fig. 3. Time profiles of A) HA titer, B) HA MW, and C) cell density in cultures of AW008 and AW009. AW008 and AW009 each coexpress *seHas* and *tuaD*, under control of the constitutive promoters P_{grac} and $P_{grac.UPmod}$, respectively, from the *amyE* locus. Cultivation conditions were the same as those described in M&M, except that glucose was the primary carbon source (20 g/L), the culture volume was 25 mL, and the inoculum size was 2% v/v. SD of experiments performed in triplicate are shown in Panels A and C, and SD of duplicate samples are shown in Panel B.

saline (NaCl, 8 g/L; KCl, 0.2 g/L; Na_2HPO_4, 1.44 g/L; KH_2PO_4, 0.24 g/L), and HA was purified with cetylpyridinium chloride as previously described (Chien and Lee, 2007a). HA titers were determined using the modified carbazole assay (Bitter and Muir, 1962), and MW was analyzed via agarose gel electrophoresis (Cowman et al., 2011) with slight modifications. 2 μg of purified HA was loaded per well, and gels stained O/N in 0.005% Stains-All (50% v/v ethanol) were destained for ~8 h in 20% v/v ethanol, followed by destaining for ~16 h in 10% v/v ethanol. Gels were then photobleached for 20 min on a LED light box, and scanned with an Epson Perfection V600 Photo scanner (Nagano, Japan). Scanned images were analyzed using ImageJ (Schneider et al., 2012), and data analysis was performed as previously described (Cowman et al., 2011). All samples were analyzed in duplicate.

2.5. Side metabolite analysis

The titers of side metabolites were analyzed via high-performance liquid chromatography (HPLC). The system consists of a Shimadzu (Kyoto, Japan) LC-10AT solvent delivery unit, Shimadzu RID-10A refractive index detector, Shimadzu CTO-20A column oven, and an Aminex HPX-87H chromatographic column (Bio-Rad Laboratories, CA). The column temperature was maintained at 65 °C, and the flow rate of the mobile phase (i.e. 5 mM H_2SO_4) was 0.6 mL/min. Signal acquisition and data processing was performed with Clarity Lite (DataApex, Prague, Czech Republic).

2.6. Real-time quantitative reverse transcription PCR (qRT-PCR)

For RNA isolation, cells were grown in the cultivation medium as described in Section 2.4 and harvested in the exponential growth phase. Total RNA was prepared using the High Pure RNA Isolation Kit (Roche Diagnostics; Basel, Switzerland) as per the manufacturer's instructions. cDNAs were synthesized using the High-Capacity cDNA Reverse Transcription Kit (ThermoFisher Scientific; MA). Sequence specific primers were used for reverse transcription of the *pfkA* (P169) mRNA, *zwf* (P171) mRNA, and internal control *rpsJ* (P173) mRNA, encoding the 30S ribosomal protein S10, at a final concentration of 1 μM. 100 ng of total RNA and 20 units of Murine RNase Inhibitor (New England Biolabs; MA) were used per 20 μL reaction. Real-time qRT-PCR was carried out using the Power SYBR® Green PCR Master Mix (ThermoFisher Scientific; MA) in an Applied Biosystems StepOnePlus™ System as per the manufacturers' instructions. Sequence specific primers were used for amplification of *pfkA* (P168/P169), *zwf* (P170/P171), and *rpsJ* (172/173). Data analysis to quantify relative expression between cultures with or without induction of dCas9 was performed as previously described (Ruijter et al., 2009). All experiments were performed in duplicate.

3. Results

3.1. Strain engineering of B. subtilis as a base strain for improved HA production

We previously constructed a *B. subtilis* strain capable of high-level production of high MW HA, i.e. AW008, in which coexpression of *seHas* and *tuaD* was driven by the strong promoter P_{grac} (Westbrook et al., 2018a). We also observed that reducing the strength of the promoter driving cardiolipin overproduction in an AW008 derivative, in which the membrane cardiolipin content was artificially enhanced, improved the HA titer by 30% with a slight reduction in the MW (Westbrook et al., 2018a). This prompted us to examine the effects of *seHas* and *tuaD* expression on HA production via construction of strain AW009, in which coexpression of both genes was driven by the promoter $P_{grac.UPmod}$, a derivative of P_{grac} with a relative promoter strength of ~0.5 (Phan et al., 2012). AW009 was constructed via transformation of *B. subtilis* 1A751 with *Nde*I-linearized pAW009 (Fig. 2). Similar to AW008, AW009 presented a mucoid phenotype, a characteristic for HA production in *B. subtilis* (Widner et al., 2005), and was genetically stable based on the persistence of the mucoid phenotype upon repetitive revival. AW009 produced approximately twice as much HA as AW008 (0.97 g/L vs. 0.48 g/L; Fig. 3A) after 10 h of shake flask cultivation, while the MW slightly declined by 12% (Fig. 3B). Moreover, the cell density of the AW009 culture at 10 h was 45% higher than that of AW008 (Fig. 3C). It is well established that the MW of HA produced in *B. subtilis* declines during extended cultivations (Westbrook et al., 2016, 2018a, 2018b; Widner et al., 2005). As our primary objective in this work was to simultaneously maximize the titer and MW of HA produced in our strains, we terminated all cultivations after 10 h. The improved cell growth of AW009, compared to AW008, may have contributed to the enhanced HA production as HA is a growth-associated product

(Huang et al., 2006). UDP-GlcNAc is the limiting substrate for HA biosynthesis in *S. zooepidemicus*, such that expression of *hasD* (a *gcaD* homologue) and/or *hasE* (a *pgi* homologue) improved the MW of HA, relative to the wild-type strain (Chen et al., 2009). Accordingly, the slight MW reduction in AW009 may have resulted from reduced expression of *tuaD*, which subsequently reduced the level of UDP-GlcUA as the limiting substrate in *B. subtilis*. With a better overall culture performance, AW009 was selected as the host for metabolic engineering via CRISPRi to enhance HA production. To conduct CRISPRi, AW009 was transformed with pAW019-2, generating AW014-2 which expressed xylose-inducible dCas9 from the *lacA* locus (Fig. 2) (Westbrook et al., 2016).

The *araE* gene encodes a broad specificity transporter of L-arabinose, D-xylose and other sugars (Krispin and Allmansberger, 1998). Expression of *araE* is not induced by xylose and is subject to CcpA-mediated catabolite repression via a catabolite repression element (CRE) upstream of the open reading frame (ORF) of *araE* (Inácio et al., 2003; Sá-Nogueira and Ramos, 1997). Given that the major carbon source for HA cultivation was sucrose (which can catabolically repress *araE* expression) and dCas9 expression was driven by the xylose-inducible promoter $P_{xylA,\ Bm}$ (Westbrook et al., 2016), we opted to integrate constitutively expressed CRE-free *araE* into the *vpr* locus of AW014-2 to enhance xylose uptake for induction of dCas9 expression. To achieve this, AW014-2 was transformed with *Sac*I-linearized pAW001-3, generating AW001-3. However, AW001-3 had a specific growth rate of approximately half that of the parent strain, indicating that expression of *araE* from $P_{grac.UPmod}$ significantly impacted cell growth. We hypothesized that such physiological burden was associated with the promoter strength and, therefore, replaced $P_{grac.UPmod}$ (with a relative promoter strength of ~0.5) with $P_{grac.\Delta UP}$ (with a relative promoter strength of ~0.1). To do this, we transformed AW014-2 with *Sac*I-linearized pAW002-3, yielding AW002-3 (Fig. 2), a strain with a specific growth rate similar to that of the parent strain.

To evaluate this approach for enhancing xylose uptake, we transformed AW002-3 with pAW018-2 (Westbrook et al., 2016), generating AW003-3, a strain that transcribed *lacZ*-gRNA.P28NT (a gRNA targeting the *lacZ* ORF of *E. coli*) from the *wprA* locus. After counter-selection to evict the P_{araE}::*mazF*-Spc^R cassette, AW003-3 was subsequently transformed with pAW016 (Westbrook et al., 2016), generating AW004-3, a strain that expressed IPTG-inducible *lacZ* from the *ugtP* locus. AW004-3 and AW016-2 (Westbrook et al., 2016), an equivalent strain to AW004-3 but without constitutively expressed *araE*, were assessed for the repression efficiency of *lacZ* expression in cultivation medium containing 2% wt/v sucrose and IPTG, in the presence or absence of xylose, as previously described (Westbrook et al., 2016). The specific β-galactosidase activities of uninduced cultures of AW004-3 and AW016-2 were 8.1-fold and 6.5-fold, respectively, that of the xylose-induced cultures of the corresponding strains (data not shown), implying less catabolite repression in AW004-3. Moreover, the 8.1-fold difference in the specific β-galactosidase activity between uninduced and xylose-induced AW004-3 grown in sucrose-containing medium compared favorably to the 7.7-fold difference in the specific β-galactosidase activity between uninduced and xylose-induced AW016-2 grown in LB (containing no sucrose) (Westbrook et al., 2016), suggesting that catabolite repression effect was insignificant in both cultures.

3.2. Repression of pfkA expression increases the HA titer but decreases the MW

Overexpressing genes in the HA biosynthetic pathway has been extensively explored for heterologous HA production in *B. subtilis*. As UDP-GlcUA is the limiting substrate in phosphate-rich medium, coexpression of *hasA*, encoding hyaluronan synthase (HasA), and *tuaD* is necessary to enhance HA production (Widner et al., 2005). However, the expression of additional genes in the HA biosynthetic pathway resulted in modest gains in the HA titer, while having essentially no effect on the MW (Jin et al., 2016; Widner et al., 2005). Accordingly, we aimed to reduce carbon flux into central metabolic pathways with the intention of increasing the availability of glucose-6-P and fructose-6-P for enhanced HA biosynthesis. We hypothesized that reducing *pfkA* expression could increase fructose-6-P levels by retarding its dissimilation via glycolysis. We recently developed a CRISPR-Cas9 toolkit for *B. subtilis* (Westbrook et al., 2016), and subsequently showed that introducing mismatches in the protospacer sequence (i.e. gRNA base-pairing region) of dCas9-targeting gRNAs and/or PAM site selection based on the relative distance from the start codon could effectively alter repression efficiency when applying CRISPRi in *B. subtilis* (Westbrook et al., 2018a). Thus, this strategy was applied in the design of seven *pfkA*-targeting gRNAs covering a range of relative repression efficiency. Single mismatches in base pairs (bp) 8–12 of the protospacer sequence (relative to the 3'-end) of gRNAs cause a dramatic (~75%) reduction in repression efficiency, while single mismatches in bp 13–20 cause a slight (~30%) reduction in repression efficiency (Note that the first 7 bp should not be altered as single mismatches in this region almost eliminate the repression efficiency.) (Larson et al., 2013; Qi et al., 2013). Moreover, repression levels are roughly inversely proportional to the distance between the selected PAM site and the start codon of the target ORF (Larson et al., 2013; Qi et al., 2013). We chose PAM sites P41NT, P315NT, and P610NT, which correspond to relative distances of 0.04, 0.33, and 0.64, respectively, from the start codon (Note that the first bp of the start codon and last bp of the stop codon correspond to relative distances of 0 and 1, respectively.). Based on proximity to the start codon alone, the relative repression efficiency afforded by targeting PAM sites P41NT, P315NT, and P610NT were estimated to be 1.0, 0.5, and 0.3, respectively (Qi et al., 2013). Single mismatches were introduced in the protospacer sequence of gRNAs at position 10 and 15 to further reduce the relative repression efficiency by ~75% and ~30%, respectively. We assumed that the effects of PAM site selection and mismatches introduced in the protospacer sequence of gRNAs were multiplicative when estimating the overall relative repression efficiency. For example, the relative repression efficiency of *pfkA* expression resulting from transcription of *pfkA*-gRNA.P41NT(10C-A) was estimated to be $1.0 \times 0.25 = 0.25$. Table 2 summarizes various *pfkA*-targeting gRNAs with their corresponding protospacer sequence and estimated relative repression efficiency.

To reduce *pfkA* expression with various repression efficiencies in HA-producing *B. subtilis*, AW002-3 was respectively transformed with *Sac*I-linearized pAW003-3, pAW004-3, pAW005-3, pAW006-3, pAW007-3, pAW008-3, and pAW009-3, generating corresponding strains AW005-3, AW006-3, AW007-3, AW008-3, AW009-3, AW010-3, and AW011-3 (Fig. 2). All *pfkA*-repressed strains produced more HA

Table 2
pfkA- and zwf-targeting gRNAs and their respective protospacer sequence and estimated relative repression efficiency.

gRNA	Protospacer sequence[a]	Relative repression efficiency
pfkA		
pfkA-gRNA.P41NT	CGAACTGCTGCGTTCATTCC	1.0
pfkA-gRNA.P41NT(10C-A)	CGAACTGCTG<u>A</u>GTTCATTCC	0.25
pfkA-gRNA.P41NT(15U-C)	CGAAC<u>C</u>GCTGCGTTCATTCC	0.7
pfkA-gRNA.P315NT(10G-A)	TAATTTTTTC<u>A</u>CACCCATAT	0.13
pfkA-gRNA.P315NT(15U-G)	TAATT<u>G</u>TTTCGCACCCATAT	0.35
pfkA-gRNA.P610NT(10G-A)	GTTCGTGGCC<u>A</u>CGTTTTAAG	0.08
pfkA-gRNA.P610NT(15U-C)	GTTCG<u>C</u>GGCCGCGTTTTAAG	0.21
zwf		
zwf-gRNA.P92NT	TTTGTCCGTTTTGATATAAA	1.0
zwf-gRNA.P92NT(10U-G)	TTTGTCCGTT<u>G</u>TGATATAAA	0.25
zwf-gRNA.P92NT(15C-A)	TTTGT<u>A</u>CGTTTTGATATAAA	0.7
zwf-gRNA.P603NT	ATGTAGCGGTTTGTCCAAAG	0.55
zwf-gRNA.P603NT(10U-C)	ATGTAGCGGT<u>C</u>TGTCCAAAG	0.14
zwf-gRNA.P603NT(15G-U)	ATGTA<u>T</u>CGGTTTGTCCAAAG	0.39

[a] Mismatches are underlined.

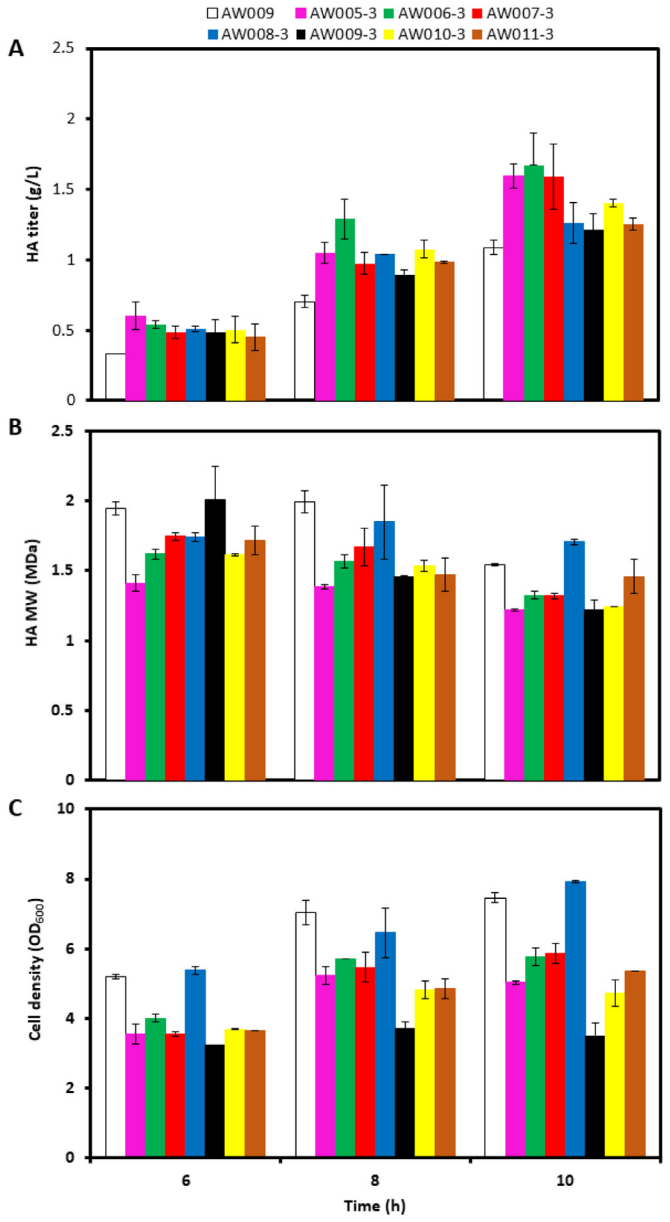

Fig. 4. Time profiles of A) HA titer, B) HA MW, and C) cell density in cultures of AW009, AW005-3 (transcribing *pfkA*-gRNA.P41NT), AW006-3 (transcribing *pfkA*-gRNA.P41NT(10C-A)), AW007-3 (transcribing *pfkA*-gRNA.P41NT(15U-C)), AW008-3 (transcribing *pfkA*-gRNA.P315NT(10G-A)), AW009-3 (transcribing *pfkA*-gRNA.P315NT(15U-G)), AW010-3 (transcribing *pfkA*-gRNA.P610NT(10G-A)), and AW011-3 (transcribing *pfkA*-gRNA.P610NT(15U-C)). All strains are derivatives of AW002-3, excluding AW009. SD of experiments performed in duplicate are shown in Panels A, B, and C.

than the control strain AW009 under shake flask cultivation (Fig. 4A). In particular, AW005-3, AW006-3, and AW007-3, which all transcribe gRNAs targeting P41NT, had HA titers ~50% higher than that of AW009 after 10 h. However, the peak and final MWs of HA produced by all *pfkA*-repressed strains were somewhat lower compared to AW009 (Fig. 4B), with the exception of AW008-3, for which the final MW was slightly higher (1.71 MDa vs. 1.54 MDa; Fig. 4B). As expected, the final cell density of *pfkA*-repressed strains was significantly lower than AW009 (Fig. 4C), with the exception of AW008-3, for which the final cell density was slightly higher (7.9 OD_{600} vs. 7.45 OD_{600}; Fig. 4C). As a result, the specific HA titers in cultures of AW005-3, AW006-3, and AW007-3 were 116%, 98%, and 86% respectively higher than that of AW009 (0.146 g/L/OD_{600}), suggesting that the dissimilated carbon flux was redirected from biomass accumulation to HA biosynthesis upon *pfkA* repression.

3.3. Repression of *zwf* expression can affect HA production

As the PPP is another central metabolic pathway potentially competing with the HA biosynthetic pathway for glucose-6-P, we hypothesized that reducing *zwf* expression could increase the availability of this key intermediate. We chose two PAM sites P92NT and P603NT, which correspond to relative distances of 0.06 and 0.41, respectively, from the start codon of the *zwf* ORF. Based on proximity to the start codon alone, the relative repression efficiency afforded by targeting PAM sites P92NT and P603NT were estimated to be 1.0 and 0.55, respectively. Single mismatches were introduced in the protospacer sequence of gRNAs at position 10 and 15 to further reduce the relative repression efficiency. Table 2 summarizes various *zwf*-targeting gRNAs with their corresponding protospacer sequences and estimated relative repression efficiencies.

To reduce *zwf* expression with various repression efficiencies in HA-producing *B. subtilis*, AW002-3 was respectively transformed with *Sac*I-linearized pAW010-3, pAW011-3, pAW012-3, pAW013-3, pAW014-3, and pAW015-3, generating corresponding strains AW012-3, AW013-3, AW014-3, AW015-3, AW016-3, and AW017-3 (Fig. 2). Culture performance for HA production for these *zwf*-repressed strains varied considerably, with the HA titers of AW012-3, AW014-3, AW015-3, and AW016-3 being 33%, 44%, 26%, and 74% respectively higher than that of AW009 after 8 h, while those of AW013-3 and AW017-3 were lower (Fig. 5A). However, HA production for AW012-3, AW014-3, AW015-3, and AW016-3 did not persist much between 8 h and 10 h, such that the final HA titers of these strains were similar to that of AW009. Moreover, the peak MW of HA produced by all *zwf*-repressed strains was somewhat lower compared to AW009, although the final MW of HA produced by AW014-3 (1.64 MDa) and AW017-3 (1.77 MDa) was higher (Fig. 5B). Also, the growth of *zwf*-repressed strains varied considerably. Cultures of AW012-3, AW013-3, and AW016-3 reached substantially lower final cell densities compared to AW009, while the final cell density in cultures of AW014-3 was a bit higher (Fig. 5C). Accordingly, the specific HA titers in cultures of AW014-3 and AW016-3 were respectively equal to and 131% higher than that of AW009.

3.4. Multiplexed repression of pfkA and zwf expression further improves the HA titer and restores the MW

We next evaluated the effect of multiplexed repression of *pfkA* and *zwf* expression on HA production. Given the significant improvements to the volumetric HA titer and, in particular, the specific HA titer in cultures of AW005-3, AW006-3, and AW016-3 compared to AW009, we selected *pfkA*-gRNA.P41NT or *pfkA*-gRNA.P41NT(10C-A) to be co-transcribed with *zwf*-gRNA.P603NT(10U-C) for gene repression in the newly derived strains. Accordingly, AW002-3 was respectively transformed with *Sac*I-linearized pAW017-3 and pAW018-3, generating corresponding strains AW018-3 and AW019-3 (Fig. 2). The HA titer in cultures of AW018-3 and AW019-3 reached 2.16 g/L and 2.26 g/L after 10 h (Fig. 6A), respectively, representing 98% and 108% increases compared to AW009. Importantly, the peak MW of HA produced by either strain was slightly higher, while the final MW in cultures of AW018-3 and AW019-3 was equal to and 14% higher, respectively, compared to AW009 (Fig. 6B). Surprisingly, the final cell density in cultures of AW018-3 (i.e. a strain with multiplexed repression of *pfkA* and *zwf*) was 53% and 88% higher, compared to AW005-3 and AW016-3 (i.e. strains with single repression of *pfkA* or *zwf*), respectively, and was slightly higher compared to AW009 (Fig. 6C). Similarly, the final cell density in cultures of AW019-3 (i.e. a strain with multiplexed repression of *pfkA* and *zwf*) was 16% and 63% higher compared to AW006-3 and AW016-3 (i.e. strains with single repression of *pfkA* or *zwf*), respectively, although was slightly lower compared to AW009.

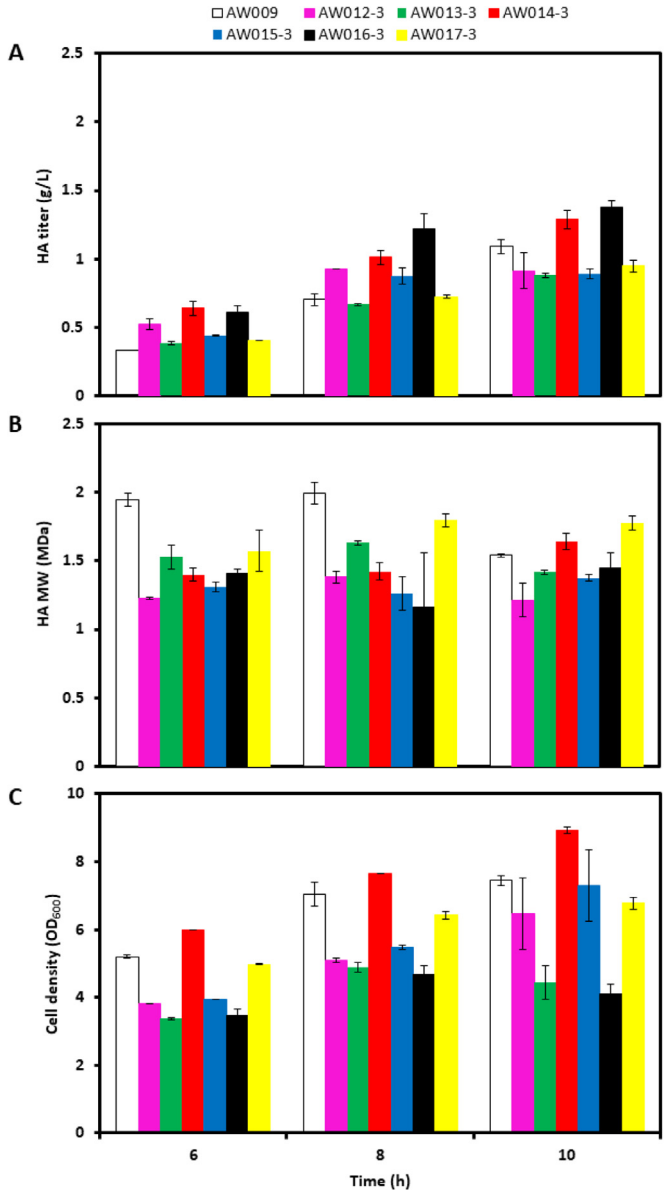

Fig. 5. Time profiles of A) HA titer, B) HA MW, and C) cell density in cultures of AW009, AW012-3 (transcribing *zwf*-gRNA.P92NT), AW013-3 (transcribing *zwf*-gRNA.P92NT(10U-G)), AW014-3 (transcribing *zwf*-gRNA.P92NT(15C-A)), AW015-3 (transcribing *zwf*-gRNA.P603NT), AW016-3 (transcribing *zwf*-gRNA.P603NT(10U-C)), and AW017-3 (transcribing *zwf*-gRNA.P603NT(15G-U)). All strains are derivatives of AW002-3, excluding AW009. SD of experiments performed in duplicate are shown in Panels A, B, and C.

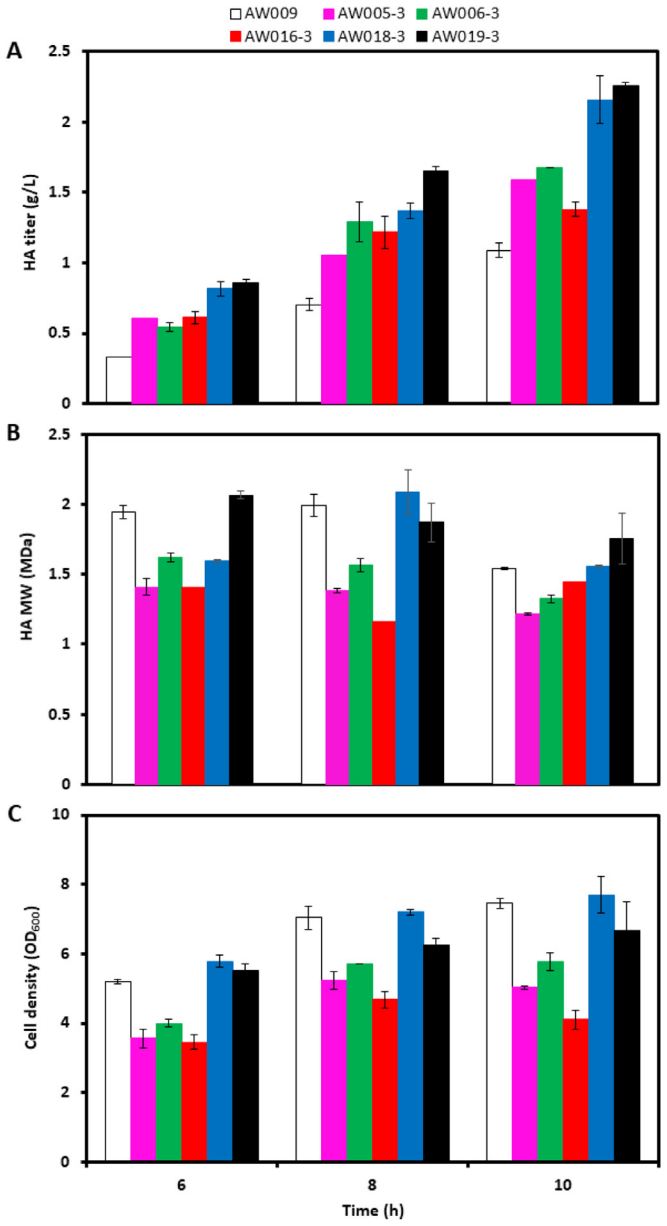

Fig. 6. Time profiles of A) HA titer, B) HA MW, and C) cell density in cultures of AW009, AW005-3 (transcribing *pfkA*-gRNA.P41NT), AW006-3 (transcribing *pfkA*-gRNA.P41NT(10C-A)), AW016-3 (transcribing *zwf*-gRNA.P603NT(10U-C)), AW018-3 (transcribing *pfkA*-gRNA.P41NT and *zwf*-gRNA.P603NT(10U-C)), and AW019-3 (transcribing *pfkA*-gRNA.P41NT(10C-A) and *zwf*-gRNA.P603NT(10U-C)). All strains are derivatives of AW002-3, excluding AW009. SD of experiments performed in duplicate are shown in Panels A, B, and C.

Accordingly, the specific HA titers in cultures of AW018-3 and AW019-3 were 92% and 131% higher after 10 h cultivation, compared to AW009. The results suggest that proper modulation of repression of *pfkA* and *zwf* expression could significantly enhance HA production without negatively affecting the MW of produced HA.

We assessed the distribution of side metabolites in cultures of AW009, AW018-3, and AW019-3 to support our hypothesis of reduced carbon dissimilation through central metabolism, resulting from repressed *pfkA* and *zwf* expression. No lactate, 2,3-butanediol, ethanol, or succinate were detected in cultures of AW009, AW018-3, and AW019-3, however, acetate and, in particular, acetoin accumulation were significant (Fig. 7). Acetate accumulation was modestly higher in cultures of AW009, compared to AW018-3 and AW019-3 (Fig. 7A), although not to the extent of impeding cell growth based on our previous experience (unpublished data). On the other hand, acetoin levels were 167% and 118% higher in cultures of AW009 after 10 h, compared to AW018-3 and AW019-3 (Fig. 7B). As acetoin can accumulate in *B. subtilis* during carbon overflow metabolism (Renna et al., 1993), the significantly lower acetoin titers in cultures of AW018-3 and AW019-3 may indicate that glycolytic carbon flux was reduced in these strains, relative to AW009.

To better understand the relationship between the repression efficiency of *pfkA* and *zwf* expression and culture performance, we assessed the transcription of these genes via qRT-PCR in 1) our control strain (i.e. AW009), 2) a strain for which culture performance was poor compared to other *pfkA*- and *zwf*- repressed strains (i.e. AW009-3 and AW012-3, respectively), and 3) strains for which culture performance was most improved compared to all other strains (i.e. AW018-3 and

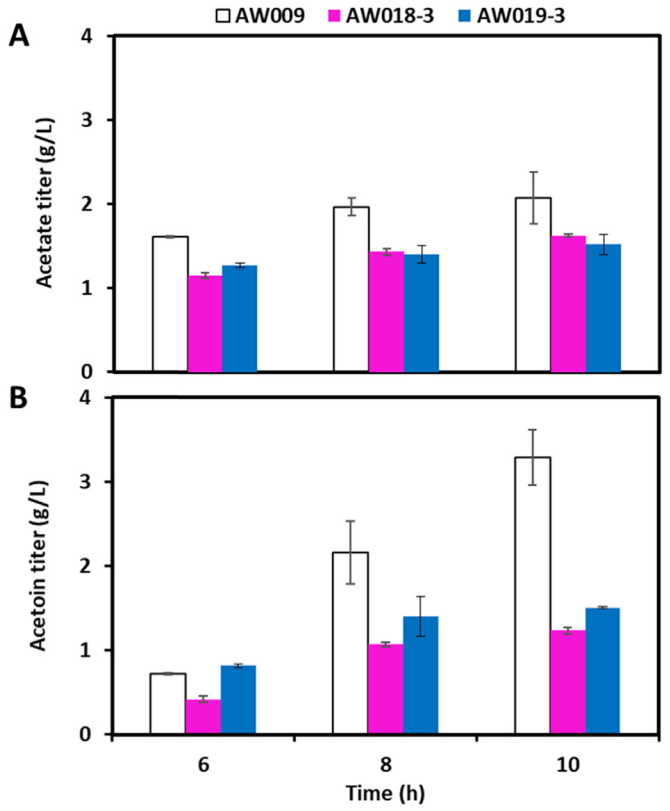

Fig. 7. Time profiles of A) acetate titer and B) acetoin titer in cultures of AW009, AW018-3 (transcribing *pfkA*-gRNA.P41NT and *zwf*-gRNA.P603NT(10U-C)), and AW019-3 (transcribing *pfkA*-gRNA.P41NT(10C-A) and *zwf*-gRNA.P603NT(10U-C)). AW018-3 and AW019-3 are derivatives of AW002-3. SD of experiments performed in duplicate are shown in Panels A and B.

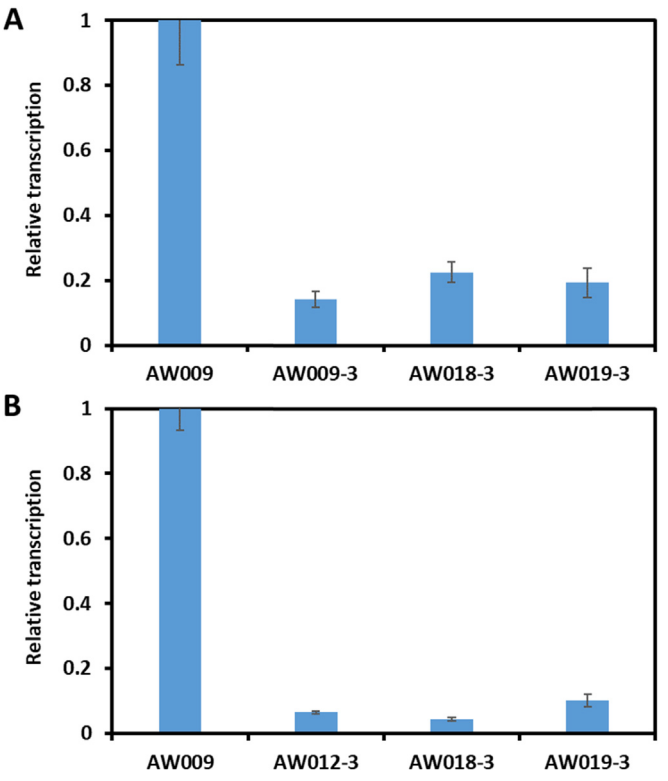

Fig. 8. Results from qRT-PCR analysis of A) *pfkA* and/or B) *zwf* transcription in AW009, AW009-3 (transcribing *pfkA*-gRNA.P315NT(15U-G)), AW012-3 (transcribing *zwf*-gRNA.P92NT), AW018-3 (transcribing *pfkA*-gRNA.P41NT and *zwf*-gRNA.P603NT(10U-C)), and AW019-3 (transcribing *pfkA*-gRNA.P41NT(10C-A) and *zwf*-gRNA.P603NT(10U-C)). All strains are derivatives of AW002-3, excluding AW009. Relative transcription (i.e. relative to the transcription of internal control *rpsJ*) was normalized to the values obtained from cultures of AW009. SD of experiments performed in duplicate are shown in Panels A and B.

AW019-3). The repression efficiency of *pfkA* transcription was high in AW009-3, AW018-3, and AW019-3, with only subtle differences observed between the three strains (Fig. 8A; note that relative transcription = 1-repression efficiency). Moreover, the observed *pfkA* transcriptional repression efficiencies did not match well with the estimated values (Table 2). For example, the respective gRNAs transcribed by AW009-3 and AW019-3, i.e. *pfkA*-gRNA.P315NT(15U-G) and *pfkA*-gRNA.P41NT(10C-A), were estimated to reduce *pfkA* transcription by ~35% and ~25% (Table 2), while the corresponding observed reductions in transcription were 86% and 81%. Similarly, the repression efficiency of *zwf* transcription was consistently high in AW012-3, AW018-3, and AW019-3 (≥ 90%; Fig. 8B), which was unexpected given that transcription of *zwf*-gRNA.P603NT(10U-C), i.e. the gRNA transcribed by both AW018-3 and AW019-3, was estimated to reduce *zwf* transcription by only 14% (Table 2). These results support our previous observation that the repression efficiencies afforded by dCas9-targeting gRNAs that contain mismatches in their protospacer sequences are difficult to anticipate (Westbrook et al., 2018a).

3.5. Supplementation of GlcNAc and GlcUA can improve the MW of HA

In this study, we attempted to redirect carbon flux from central metabolism, i.e. the PPP and glycolysis, toward HA biosynthesis by repressing expression of *zwf* and/or *pfkA*, which encode branch point enzymes driving dissimilated carbon into the respective pathways. Significant improvements to the HA titer were obtained in cultures of all seven AW002-3 derivatives transcribing *pfkA*-targeting gRNAs covering a range of relative repression efficiency (Fig. 4A). Note that *pfkA* is an essential gene in *B. subtilis* (Fischer and Sauer, 2005; Kobayashi et al., 2003) that cannot be knocked out, and repression of *pfkA* expression should reduce glycolytic carbon flux. Our results are consistent with a previous study in which attenuated *pfkA* expression via start codon replacement improved the HA titer in *B. subtilis* (Jin et al., 2016). However, the increase in the HA titer was accompanied by a decrease in the MW (Fig. 4B). HA biosynthesis is limited by insufficient UDP-GlcNAc levels in *S. zooepidemicus* (Chen et al., 2009), such that overexpression of *hasE* and *hasD* (i.e. respective homologues of *pgi* and *gcaD* encoding enzymes involved in UDP-GlcNAc synthesis) (Chen et al., 2009), or addition of exogenous GlcNAc (Jagannath and Ramachandran, 2010) dramatically improved the MW. A similar substrate imbalance could exist with UDP-GlcUA being the limiting substrate for HA biosynthesis in *B. subtilis* under our cultivation conditions (i.e. using a medium with a high phosphate content), potentially causing premature termination of the growing HA polymer (Chen et al., 2009). Theoretically, overexpression of *tuaD* should at least partially resolve the natural imbalance between UDP-GlcUA and UDP-GlcNAc. However, we suspected that the reduced expression of *pfkA* might have increased the conversion of fructose-6-P to glucosamine-6-P via GlmS and, therefore, increased the carbon dissimilation through the UDP-GlcNAc branch of the HA biosynthetic pathway, resulting in an imbalance between substrate levels and a reduction in the MW.

To test this hypothesis, we supplemented cultures of AW006-3 with either GlcUA or GlcNAc at a concentration of 0.4 g/L or 0.8 g/L. Interestingly, the addition of GlcUA and GlcNAc to 0.4 g/L reduced the final HA titer by 31% and 55%, respectively, compared to cultures without exogenous GlcUA and GlcNAc, while increasing the concentration of each substrate to 0.8 g/L led to respective 18% and 24% increases in the final HA titer, compared to the corresponding cultures

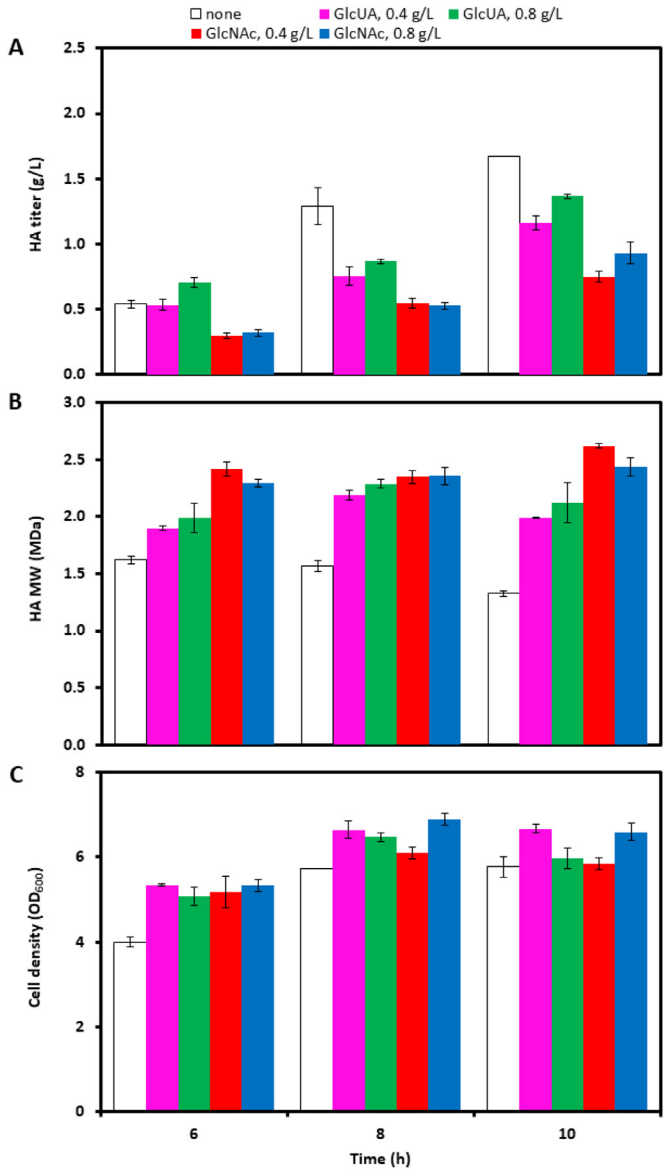

Fig. 9. Time profiles of A) HA titer, B) HA MW, and C) cell density in cultures of AW006-3, an AW002-3 derivative transcribing *pfkA*-gRNA.P41NT(10C-A), supplemented with GlcUA or GlcNAc at a concentration of 0.4 g/L or 0.8 g/L. SD of experiments performed in duplicate are shown in Panels A and B.

with a concentration of 0.4 g/L (Fig. 9A). Moreover, the addition of 0.4 g/L GlcUA resulted in a 35% increase in the peak MW (2.19 MDa; at 8 h), compared to the peak MW (1.62 MDa; at 6 h) of the control culture lacking exogenous supplementation (Fig. 9B). The effect on MW was even more pronounced in the culture supplemented with 0.4 g/L GlcNAc, and the peak MW reached 2.62 MDa at 10 h, representing a 62% increase compared to the control culture (Fig. 9B). A further increase in the concentration of either substrate to 0.8 g/L had a marginal effect on the MW, compared to the corresponding culture with a concentration of 0.4 g/L (Fig. 9B). The decrease in the HA titer without cell growth being negatively affected upon the addition of exogenous GlcUA or GlcNAc may suggest that imbalanced substrate levels occurred even at the lowest concentration of 0.4 g/L.

4. Discussion

HA biosynthesis is a metabolically demanding process, requiring 2 mol glucose, 3 mol ATP, 2 mol UTP, and 1 mol acetyl-CoA to generate 1 mol of the HA disaccharide. The major substrates for HA biosynthesis, i.e. nucleotide sugars UDP-GlcUA and UDP-GlcNAc, are also required for cell wall biosynthesis. Hence, HA biosynthesis directly competes with the PPP and glycolysis for glucose-6-P and fructose-6-P, respectively. However, heterologous HA production in *B. subtilis* often does not significantly alter the cell growth profile based on our observations (unpublished data) and others (Widner et al., 2005), suggesting that an autonomously balanced substrate allocation can exist between central metabolism and biosynthesis of HA and cell wall. Accordingly, overexpressing enzymes involved in HA biosynthesis may be futile, particularly if substrate availability is the limiting factor due to strict carbon flux partitioning in the HA-producing host.

The standard approach to metabolic engineering has been to overexpress genes in the biosynthetic pathway leading to target metabolite formation, while mutating genes to inactivate pathways that generate side metabolites (Lee et al., 2012). As previously mentioned, the upregulation of genes comprising the HA biosynthetic pathway in *B. subtilis*, beyond those encoding prerequisite enzymes HasA and TuaD, results in modest improvements (at best) to culture performance (Jin et al., 2016; Widner et al., 2005), which we have also confirmed in this study by overexpressing *pgcA* and/or *glmS* in AW009 as discussed later. Here, we implement a novel approach of reducing carbon dissimilation through central metabolism to enhance HA production in *B. subtilis* by reducing the expression of *pfkA* and *zwf*, respectively encoding enzymes at the branchpoints of glycolysis and the PPP with cell wall biosynthesis, via CRISPRi. The reduced expression of *pfkA* was demonstrated to enhance HA production in *B. subtilis* (Jin et al., 2016), although their strategy was to replace the start codon of the *pfkA* ORF. This approach is more tedious to implement, from the perspective of strain construction, and obviously less versatile as only two possible alternate codons are available, severely limiting the range of gene expression that can be achieved. In our study, acetate and acetoin were the major side metabolites observed in cultures of AW009 (Fig. 7). Abolishing acetate formation in *B. subtilis* necessitates disruption of the pyruvate dehydrogenase complex (Li et al., 2012), which starves the TCA cycle of acetyl-CoA and, in turn, severely diminishes ATP production. Given that HA biosynthesis is an ATP-intensive process, inactivating the pyruvate dehydrogenase complex is likely not a suitable approach to enhance HA production in *B. subtilis*. Moreover, we have observed that attempting to abolish acetoin production via mutation of *alsD*, encoding 2-acetolactate decarboxylase (AlsD), hinders culture performance in *B. subtilis* strains engineered for L-valine overproduction from sucrose (unpublished data). On the other hand, our novel metabolic engineering strategy of reducing *pfkA* and *zwf* expression appears to favor the redistribution of dissimilated carbon from side metabolite formation toward HA biosynthesis, as demonstrated by the significantly improved specific HA titers, and reduced acetate and acetoin accumulation in cultures of AW018-3 and AW019-3, compared to AW009.

The activity of membrane-bound SeHAS was observed to decrease with increasing UDP-GlcUA concentration, particularly when the ratio of UDP-GlcUA to UDP-GlcNAc was significantly higher than 1:1 (Tlapak-Simmons et al., 1999). While a proposed decline in the activity of SeHAS may seem counterintuitive given the large increase in the MW observed upon the addition of either GlcUA or GlcNAc in our study (Fig. 8B), note that the polymerizing activity (affecting HA titer) and control of chain length (affecting HA MW) are independent functions of SeHAS that are not necessarily coupled to each other (Weigel and Baggenstoss, 2012). On the other hand, in the presence of excess UDP-GlcUA or UDP-GlcNAc, chain elongation might stall temporarily as the excess substrate transiently occupies the binding site of the other substrate as a competitive inhibitor (Tlapak-Simmons et al., 1999), but the chain is retained until the appropriate substrate is available for synthesis and chain elongation to commence. An alternate explanation might be that supplementing cultures with GlcNAc altered the rate of synthesis of UDP-GlcNAc. GlcNAc is simultaneously transported into the cell and phosphorylated to yield GlcNAc-6-P by the GlcNAc specific

phosphotransferase system transporter NagP, and GlcNAc-6-P is subsequently converted to glucosamine-6-P by GlcNAc-6-P deacetylase (i.e. NagA) (Gaugué et al., 2013). Glucosamine-6-P inhibits expression of *glmS* by associating with its 5'-untranslated region (UTR), resulting in self-cleavage of the 5'-UTR by the *glmS* ribozyme, and subsequent targeting of the *glmS* mRNA for degradation (Collins et al., 2007). Accordingly, the addition of exogenous GlcNAc in cultures of AW006-3 may disrupt the dissimilated carbon flux into the UDP-GlcNAc branch of the HA biosynthetic pathway and, therefore, increase the ratio of UDP-GlcUA to UDP-GlcNAc, resulting in decreased HA titers and increased MWs. We have previously observed that increased HA titers in cultures of *B. subtilis* are often accompanied by a decrease in the MW (Westbrook et al., 2018a), and the yield on glucose and MW of HA produced in *S. zooepidemicus* were not correlated (Chen et al., 2009). In any case, further investigation is required to elucidate the effects of overall carbon flux into the HA biosynthetic pathway and the UDP-GlcNAc/UDP-GlcUA ratio on the titer and MW of HA produced in *B. subtilis*.

The culture performance of *zwf*-repressed strains varied considerably. Mutation of *zwf* resulted in increased glycolytic flux in *B. subtilis* grown on glucose, albeit with a lower biomass yield (Fischer and Sauer, 2005). This is consistent with our results as the final cell density of all *zwf*-repressed strains except AW014-3 was lower compared to AW009 (Fig. 5C). Clearly, the majority of carbon diverted from the PPP either entered glycolysis or another pathway other than HA biosynthesis given that the HA titers were not necessarily increased in these *zwf*-repressed strains (Fig. 5A). In this context, improving HA production may not be possible without reducing *pfkA* expression, particularly when the primary carbon source is sucrose with half of the dissimilated carbon naturally bypassing Zwf. By simultaneously repressing the expression of both *pfkA* and *zwf* in AW018-3 and AW019-3, we obtained significant increases in the HA titer (Fig. 6A) and modest enhancements to the MW relative to AW009 (Fig. 6B), indicating a significantly higher and more balanced carbon flux through the UDP-GlcUA and UDP-GlcNAc branches for HA biosynthesis. Note that the high degree of reversibility for the interconversion of glucose-6-P and fructose-6-P by Pgi is well documented (Gombert et al., 2001; Wittmann and De Graaf, 2005), potentially leading to more balanced flux distribution at these two nodes toward UDP-GlcUA and UDP-GlcNAc, respectively, in AW018-3 and AW019-3.

To test the efficacy of overexpressing genes in either branch of the HA biosynthetic pathway to enhance culture performance, we transformed AW009 with *Sac*I-linearized pAW019-3, *Sca*I-linearized-pAW020-3, and *Sca*I-linearized-pAW021-3, generating corresponding strains AW020-3, AW021-3, and AW022-3, which overexpressed *pgcA*, *glmS*, or both genes from the *thrC* locus, respectively. The titers and MWs of HA produced in cultures of AW020-3, AW021-3, and AW022-3 were highly similar to those obtained in cultures of AW009 (data not shown), confirming the deficiency of this metabolic approach.

In addition to *pfkA* and *zwf*, we also targeted additional essential genes of interest for transcriptional interference, i.e. *tagO*, encoding UDP-GlcNAc-undecaprenyl-phosphate *N*-acetylglucosaminephosphotransferase (TagO) that converts UDP-GlcNAc to *N*-acetyl-glucosaminyldiphospho-*ditrans,octacis*-undecaprenol during teichoic acid synthesis, and *murAA*, encoding UDP-GlcNAc 1-carboxyvinyltransferase (MurAA) that converts UDP-GlcNAc to UDP-GlcNAc-enolpyruvate during UDP-N-acetylmuramoyl-pentapeptide (i.e. cell wall) synthesis (Fig. 1) (Kobayashi et al., 2003). However, preliminary attempts to reduce the expression of *tagO* and *murAA* via CRISPRi in AW002-3 resulted in poor growth and genetic instability, as certain derived *B. subtilis* strains lost the mucoid phenotype for HA production (data not shown). Accordingly, future attempts to repress expression of these genes may employ very low levels of repression.

While the feasibility of repressing the expression of *pfkA* and *zwf* for enhanced HA production has been demonstrated, our results indicate that anticipating the repression efficiency afforded by dCas9-targeting gRNAs is difficult, particularly when mismatches have been introduced in the protospacer sequence. Our observation of a high repression efficiency of *pfkA* and *zwf* transcription in AW019-3, which transcribed two gRNAs with mismatches at position 10 of the protospacer sequence (i.e. *pfkA*-gRNA.P41NT(10C-A) and *zwf*-gRNA.P603NT(10U-C)), is in agreement with our previous work in which a gRNA targeting the *ftsZ* ORF that contained a mismatch at position 10 of the protospacer sequence provided a significantly higher than expected repression efficiency (Westbrook et al., 2018a). These observations were unexpected given that the 12 bp from the 3' end of the protospacer sequence were reported to comprise a seed region in which mutations severely hampered repression efficiency (Qi et al., 2013), although the results of this study and our prior work suggest that certain mutations can be tolerated in this region of the protospacer sequence. Moreover, a correlation between the repression efficiency of *pfkA* and *zwf* expression and culture performance for HA production is not evident, as only subtle differences in the transcription levels of each gene were observed between respective strains for which the culture performance was poorest (i.e. AW009-3 and AW012-3) and most improved (i.e. AW018-3 and AW019-3). Accordingly, anticipating the effects of altered repression efficiency for the expression of target genes may not be practical, such that the design of multiple gRNAs for a single target is deemed necessary to realize the true impact of its repression on target metabolite production. Nevertheless, our results stress the importance of balancing intracellular substrate levels of UDP-GlcUA and UDP-GlcNAc for high-level production of high-MW HA in engineered *B. subtilis*.

Appendix A. Supplementary material

Supplementary data associated with this article can be found in the online version at http://dx.doi.org/10.1016/j.ymben.2018.04.016.

References

Bitter, T., Muir, H.M., 1962. A modified uronic acid carbazole reaction. Anal. Biochem. 4, 330–334.

Chen, W.Y., Marcellin, E., Hung, J., Nielsen, L.K., 2009. Hyaluronan molecular weight is controlled by UDP-N-acetylglucosamine concentration in *Streptococcus zooepidemicus*. J. Biol. Chem. 284, 18007–18014.

Cheng, F., Luozhong, S., Guo, Z., Yu, H., Stephanopoulos, G., 2017. Enhanced biosynthesis of hyaluronic acid using engineered Corynebacterium glutamicum via metabolic pathway regulation. Biotechnol. J. 12.

Chien, L.-J., Lee, C.-K., 2007a. Enhanced hyaluronic acid production in *Bacillus subtilis* by coexpressing bacterial hemoglobin. Biotechnol. Prog. 23, 1017–1022.

Chien, L.-J., Lee, C.-K., 2007b. Hyaluronic acid production by recombinant *Lactococcus lactis*. Appl. Microbiol. Biotechnol. 77, 339–346.

Collins, J.A., Irnov, I., Baker, S., Winkler, W.C., 2007. Mechanism of mRNA destabilization by the *glmS* ribozyme. Genes Dev. 21, 3356–3368.

Cowman, M.K., Chen, C.C., Pandya, M., Yuan, H., Ramkishun, D., LoBello, J., Bhilocha, S., Russell-Puleri, S., Skendaj, E., Mijovic, J., Jing, W., 2011. Improved agarose gel electrophoresis method and molecular mass calculation for high molecular mass hyaluronan. Anal. Biochem. 417, 50–56.

Desai, R.P., Papoutsakis, E.T., 1999. Antisense RNA strategies for metabolic engineering of *Clostridium acetobutylicum*. Appl. Environ. Microbiol. 65, 936–945.

Fischer, E., Sauer, U., 2005. Large-scale in vivo flux analysis shows rigidity and suboptimal performance of *Bacillus subtilis* metabolism. Nat. Genet. 37, 636–640.

Gaugué, I., Oberto, J., Putzer, H., Plumbridge, J., 2013. The use of amino sugars by *Bacillus subtilis*: presence of a unique operon for the catabolism of glucosamine. PLoS One 8, e63025.

Goa, K., Benfield, P., 1994. Hyaluronic acid. Drugs 47, 536–566.

Gombert, A.K., dos Santos, M.M., Christensen, B., Nielsen, J., 2001. Network identification and flux quantification in the central metabolism of *Saccharomyces cerevisiae* under different conditions of glucose repression. J. Bacteriol. 183, 1441–1451.

Harwood, C.R., Cutting, S.M., 1990. Molecular Biological Methods for *Bacillus*. Wiley, Chichester; New York.

Huang, W.-C., Chen, S.-J., Chen, T.-L., 2006. The role of dissolved oxygen and function of agitation in hyaluronic acid fermentation. Biochem. Eng. J. 32, 239–243.

Inácio, J.M., Costa, C., de Sá-Nogueira, I., 2003. Distinct molecular mechanisms involved in carbon catabolite repression of the arabinose regulon in *Bacillus subtilis*. Microbiology 149, 2345–2355.

Jagannath, S., Ramachandran, K., 2010. Influence of competing metabolic processes on the molecular weight of hyaluronic acid synthesized by *Streptococcus zooepidemicus*. Biochem. Eng. J. 48, 148–158.

Jia, Y., Zhu, J., Chen, X., Tang, D., Su, D., Yao, W., Gao, X., 2013. Metabolic engineering of *Bacillus subtilis* for the efficient biosynthesis of uniform hyaluronic acid with controlled molecular weights. Bioresour. Technol. 132, 427–431.

Jin, P., Kang, Z., Yuan, P., Du, G., Chen, J., 2016. Production of specific-molecular-weight hyaluronan by metabolically engineered *Bacillus subtilis* 168. Metab. Eng. 35, 21–30.
Keasling, J.D., 2010. Manufacturing molecules through metabolic engineering. Science 330, 1355–1358.
Kobayashi, K., Ehrlich, S.D., Albertini, A., Amati, G., Andersen, K.K., Arnaud, M., Asai, K., Ashikaga, S., Aymerich, S., Bessieres, P., Boland, F., Brignell, S.C., Bron, S., Bunai, K., Chapuis, J., Christiansen, L.C., Danchin, A., Débarbouillé, M., Dervyn, E., Deuerling, E., Devine, K., Devine, S.K., Dreesen, O., Errington, J., Fillinger, S., Foster, S.J., Fujita, Y., Galizzi, A., Gardan, R., Eschevins, C., Fukushima, T., Haga, K., Harwood, C.R., Hecker, M., Hosoya, D., Hullo, M.F., Kakeshita, H., Karamata, D., Kasahara, Y., Kawamura, F., Koga, K., Koski, P., Kuwana, R., Imamura, D., Ishimaru, M., Ishikawa, S., Ishio, I., Le Coq, D., Masson, A., Mauël, C., Meima, R., Mellado, R.P., Moir, A., Moriya, S., Nagakawa, E., Nanamiya, H., Nakai, S., Nygaard, P., Ogura, M., Ohanan, T., O'Reilly, M., O'Rourke, M., Pragai, Z., Pooley, H.M., Rapoport, G., Rawlins, J.P., Rivas, L.A., Rivolta, C., Sadaie, A., Sadaie, Y., Sarvas, M., Sato, T., Saxild, H.H., Scanlan, E., Schumann, W., Seegers, J.F.M.L., Sekiguchi, J., Sekowska, A., Séror, S.J., Simon, M., Stragier, P., Studer, R., Takamatsu, H., Tanaka, T., Takeuchi, M., Thomaides, H.B., Vagner, V., van Dijl, J.M., Watabe, K., Wipat, A., Yamamoto, H., Yamamoto, M., Yamamoto, Y., Yamane, K., Yata, K., Yoshida, K., Yoshikawa, H., Zuber, U., Ogasawara, N., 2003. Essential *Bacillus subtilis* genes. Proc. Natl. Acad. Sci. USA 100, 4678–4683.
Kogan, G., Šoltés, L., Stern, R., Gemeiner, P., 2007. Hyaluronic acid: a natural biopolymer with a broad range of biomedical and industrial applications. Biotechnol. Lett. 29, 17–25.
Krispin, O., Allmansberger, R., 1998. The *Bacillus subtilis* AraE protein displays a broad substrate specificity for several different sugars. J. Bacteriol. 180, 3250–3252.
Larson, M.H., Gilbert, L.A., Wang, X., Lim, W.A., Weissman, J.S., Qi, L.S., 2013. CRISPR interference (CRISPRi) for sequence-specific control of gene expression. Nat. Protoc. 8, 2180–2196.
Lee, J.W., Na, D., Park, J.M., Lee, J., Choi, S., Lee, S.Y., 2012. Systems metabolic engineering of microorganisms for natural and non-natural chemicals. Nat. Chem. Biol. 8, 536–546.
Li, S., Huang, D., Li, Y., Wen, J., Jia, X., 2012. Rational improvement of the engineered isobutanol-producing Bacillus subtilis by elementary mode analysis. Microb. Cell Factor. 11, 101.
Liu, L., Liu, Y., Li, J., Du, G., Chen, J., 2011. Microbial production of hyaluronic acid: current state, challenges, and perspectives. Microb. Cell Factor. 10, 99.
Mao, Z., Chen, R.R., 2007. Recombinant synthesis of hyaluronan by *Agrobacterium* sp. Biotechnol. Prog. 23, 1038–1042.
Mao, Z., Shin, H.-D., Chen, R., 2009. A recombinant *E. coli* bioprocess for hyaluronan synthesis. Appl. Microbiol. Biotechnol. 84, 63–69.
Nguyen, H., Phan, T., Schumann, W., 2007. Expression vectors for the rapid purification of recombinant proteins in *Bacillus subtilis*. Curr. Microbiol. 55, 89–93.
Phan, T.T.P., Nguyen, H.D., Schumann, W., 2012. Development of a strong intracellular expression system for *Bacillus subtilis* by optimizing promoter elements. J. Biotechnol. 157, 167–172.
Prasad, S., Jayaraman, G., Ramachandran, K.B., 2010. Hyaluronic acid production is enhanced by the additional co-expression of UDP-glucose pyrophosphorylase in *Lactococcus lactis*. Appl. Microbiol. Biotechnol. 86, 273–283.
Qi, Lei S., Larson, Matthew, H., Gilbert, Luke, A., Doudna, Jennifer, A., Weissman, Jonathan, S., Arkin, Adam, P., Lim, Wendell, A., 2013. Repurposing CRISPR as an RNA-guided platform for sequence-specific control of gene expression. Cell 152, 1173–1183.
Renna, M.C., Najimudin, N., Winik, L., Zahler, S., 1993. Regulation of the Bacillus subtilis alsS, alsD, and alsR genes involved in post-exponential-phase production of acetoin. J. Bacteriol. 175, 3863–3875.
Ruijter, J.M., Ramakers, C., Hoogaars, W.M.H., Karlen, Y., Bakker, O., van den Hoff, M.J.B., Moorman, A.F.M., 2009. Amplification efficiency: linking baseline and bias in the analysis of quantitative PCR data. Nucleic Acids Res. 37, e45.
Sá-Nogueira, I., Ramos, S.S., 1997. Cloning, functional analysis, and transcriptional regulation of the *Bacillus subtilis araE* gene involved in L-arabinose utilization. J. Bacteriol. 179, 7705–7711.
Sambrook, J., Russell, D., 2001. Molecular Cloning: A Laboratory Manual. Cold Spring Harbor Laboratory Press, Cold Spring Harbor, New York.
Schallmey, M., Singh, A., Ward, O.P., 2004. Developments in the use of *Bacillus* species for industrial production. Can. J. Microbiol. 50, 1–17.
Schneider, C.A., Rasband, W.S., Eliceiri, K.W., 2012. NIH Image to ImageJ: 25 years of image analysis. Nat. Methods 9, 671–675.
Tlapak-Simmons, V.L., Baggenstoss, B.A., Kumari, K., Heldermon, C., Weigel, P.H., 1999. Kinetic characterization of the recombinant hyaluronan synthases from *Streptococcus pyogenes* and *Streptococcus equisimilis*. J. Biol. Chem. 274, 4246–4253.
Weigel, P.H., Baggenstoss, B.A., 2012. Hyaluronan synthase polymerizing activity and control of product size are discrete enzyme functions that can be uncoupled by mutagenesis of conserved cysteines. Glycobiology 22, 1302–1310.
Weigel, P.H., Hascall, V.C., Tammi, M., 1997. Hyaluronan synthases. J. Biol. Chem. 272, 13997–14000.
Weissmann, B., Meyer, K., 1954. The structure of hyalobiuronic acid and of hyaluronic acid from umbilical Cord1, 2. J. Am. Chem. Soc. 76, 1753–1757.
Westbrook, A.W., Moo-Young, M., Chou, C.P., 2016. Development of a CRISPR-Cas9 tool kit for comprehensive engineering of *Bacillus subtilis*. Appl. Environ. Microbiol. 82, 4876–4895.
Westbrook, A.W., Ren, X., Moo-Young, M., Chou, C.P., 2018a. Engineering of cell membrane to enhance heterologous production of hyaluronic acid in *Bacillus subtilis*. Biotechnol. Bioeng. 115, 216–231.
Westbrook, A.W., Ren, X., Moo-Young, M., Chou, C.P., 2018b. Application of hydrocarbon and perfluorocarbon oxygen vectors to enhance heterologous production of hyaluronic acid in engineered Bacillus subtilis. Biotechnol. Bioeng.
Widner, B., Behr, R., Von Dollen, S., Tang, M., Heu, T., Sloma, A., Sternberg, D., DeAngelis, P.L., Weigel, P.H., Brown, S., 2005. Hyaluronic acid production in *Bacillus subtilis*. Appl. Environ. Microbiol. 71, 3747–3752.
Wittmann, C., De Graaf, A., 2005. Metabolic flux analysis in *Corynebacterium glutamicum*. In: Eggeling, L., Bott, M. (Eds.), Handbook of *Corynebacterium glutamicum*. CRC, Taylor & Francis, Boca Raton, FL, pp. 277–300.
Wolf, M., Geczi, A., Simon, O., Borriss, R., 1995. Genes encoding xylan and β-glucan hydrolysing enzymes in *Bacillus subtilis*: characterization, mapping and construction of strains deficient in lichenase, cellulase and xylanase. Microbiology 141, 281–290.
Yoshimura, T., Shibata, N., Hamano, Y., Yamanaka, K., 2015. Heterologous production of hyaluronic acid in an ε-poly-L-lysine producer, *Streptomyces albulus*. Appl. Environ. Microbiol. 81, 3631–3640.
Yu, H., Stephanopoulos, G., 2008. Metabolic engineering of *Escherichia coli* for biosynthesis of hyaluronic acid. Metab. Eng. 10, 24–32.